LUND UNIVERSITY

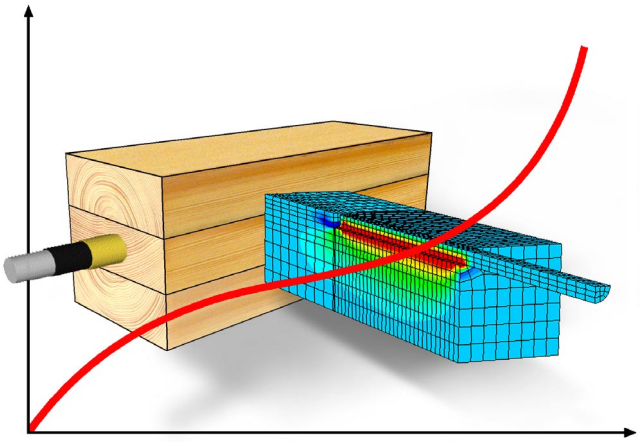

STRENGTH AND CREEP ANALYSIS OF GLUED RUBBER FOIL TIMBER JOINTS

HENRIK DANIELSSON
and PETER BJÖRNSSON

Structural Mechanics

Master's Dissertation

Structural Mechanics

ISRN LUTVDG/TVSM--05/5137--SE (1-93)
ISSN 0281-6679

STRENGTH AND CREEP ANALYSIS OF GLUED RUBBER FOIL TIMBER JOINTS

Master's Dissertation by

Peter Björnsson and Henrik Danielsson

Supervisors:

Per Johan Gustafsson, Erik Serrano, and
Per-Erik Austrell, Div. of Structural Mechanics

Printed by KFS I Lund AB, Lund, Sweden, December, 2005.

For information, address:
Division of Structural Mechanics, LTH, Lund University, Box 118, SE-221 00 Lund, Sweden.
Homepage: http://www.byggmek.lth.se

Abstract

In this master's thesis, the possibility of increasing the load bearing capacity of glued timber joints by the use of a rubber foil was investigated. A rubber foil is believed to ensure a more uniform distribution of stresses and thereby greater load bearing capacity.

The work within this master's thesis consisted of developing material models for rubber based on experimental tests in order to enable analyses of interesting applications. Results from finite element analyses indicate an almost uniform shear stress distribution along a glued in rod, both at short term and long term loading.

Keywords: Timber joint, glue joint, glued in rod, rubber foil, stress distribution, hyperelasticity, viscoelasticity, FEM, finite element analysis.

Acknowledgements

This master's thesis study was carried out during the fall of 2005 at the Division of Structural Mechanics at Lund University, Sweden.

We would first of all like to express our sincere gratitude to our supervisors Prof. Per Johan Gustafsson and Dr. Erik Serrano for their guidance and support. We are also grateful to Mr. Thord Lundgren for useful help during experimental testing, Dr. Per Erik Austrell for consultation concerning rubber, Mr. Magnus Wikström for supplying experimental test data, Mr. Bo Zadig for helping us with graphics and printing and also the rest of the staff at the Division of Structural Mechanics for helping us out during the work of this thesis.

Lund, December 2005

Peter Björnsson Henrik Danielsson

Summary

This master's thesis concerns glued rubber foil timber joints. In conventionally glued timber joints, the load bearing capacity is in most cases limited by large stress concentrations in the adhesive bond. The idea of using a rubber foil in glued timber joints is based on the expected ability of rubber to give a more uniform distribution of stresses and thereby increase the load bearing capacity. The concept of using a rubber foil in glued timber joints is rather new and still in the research stage.

The aim of the study was to develop material models for rubber in order to enable deformation and strength analyses of interesting applications. In the work of investigating material properties and developing material models, experimental tests were made. In order to determine the hyperelastic stress vs. strain relationship, a short term ramped loading test of the rubber in simple shear was carried out. The viscoelastic properties were determined by experimental creep tests with different constant load levels. The obtained material parameters, describing the properties of the used rubber, were then calibrated in finite element analyses of the same experimental tests. As the last step of the development of material models, the calibrated parameters were verified in finite element analyses of other experimental tests. Having achieved reliable material models, finite element analyses of a glued in rod with a rubber foil were performed for short- and long term loading. The results were then analysed and the effect of using a rubber foil was evaluated.

The results of the short term analyses show that the expectation on the ability of the rubber foil to distribute stresses is well founded. A comparison between the stress distribution in the rubber foil joint and a typical stress distribution of the same type of joint without the rubber foil show a significant difference. The fact that the rubber distributes the stresses well means that the glued in length has only a small influence on the relative load bearing capacity of a glued in rod joint.

In the analyses with long term loading, the time dependency of the load bearing capacity was studied. The results show that the decrease in capacity due to long duration of the load may be significant. It is also suggested that the decrease in capacity can be described by the relaxation modulus for a rubber with a fairly linear stress vs. strain relationship.

Another conclusion is that the rubber needs to be strong enough to make the capacity of the joint dependent on the strength of the adhesive bond rather than the rubber foil. If this is the case, full advantage of the rubber's ability to distribute stresses is taken and the load bearing capacity can be increased substantially compared to a conventionally glued joint.

Sammanfattning

Detta examensarbete behandlar limmade gummifolieförband i träkonstruktioner. I konventionellt limmade träförband är lastkapaciteten vanligtvis begränsad av spänningskoncentrationer i limskiktet. Idén med att använda en gummifolie i limmade träförband baseras på gummits förväntade förmåga att ge en jämnare spänningsfördelning och därmed ökad bärförmåga. Konceptet att använda en gummifolie i limmade träförband är relativt nytt och fortfarande i forskningsstadiet.

Målet med studien var att utveckla materialmodeller för gummi för att möjliggöra deformations- och styrkeanalyser av intressanta tillämpningar. Under arbetet med att undersöka materialegenskaper och utveckla materialmodeller utfördes experimentella tester. För att bestämma det hyperelastiska spännings-töjningssambandet utfördes ett korttidsförsök med ökande last i enkel skjuvning. De viskoelastiska egenskaperna bestämdes utifrån kryptester med olika konstanta lastnivåer. Erhållna materialparametrar som beskriver gummits egenskaper kalibrerades därefter genom finita elementanalyser av de experimentella testerna. Det sista steget i utvecklingen av materialmodeller bestod av att verifiera de kalibrerade parametrarna genom finita element analyser av andra experimentella tester. När tillförlitliga materialmodeller hade tagits fram utfördes finita elementanalyser av en inlimmad stång med gummifolie för kort- och långtidslast. Därefter analyserades resultaten och effekten av att använda en gummifolie utvärderades.

Resultaten av korttidsanalyserna visar att förväntningen på gummits förmåga att fördela spänningar är väl grundad. En jämförelse mellan spänningsfördelningarna för gummiefolieförbandet och för samma sorts förband utan gummifolie visar en markant skillnad. Det faktum att gummit fördelar spänningarna väl innebär att den inlimmade längden endast har ett litet inflytande på den relativa lastkapaciteten hos en inlimmad stång.

I analyserna med långtidsbelastning studerades lastkapacitetens tidsberoende. Resultaten visar att minskningen av kapaciteten på grund av långvarig last kan vara betydlig. Det visas även att minskningen av kapaciteten för ett gummi med någorlunda linjärt spännings-töjningssamband kan beskrivas av relaxationsmodulen för materialet.

En annan slutsats är att gummit bör vara tillräckligt starkt för att förbandets lastkapacitet ska vara beroende av limmets styrka snarare än gummits styrka. Om gummit är starkare än limmet utnyttjas gummits förmåga att fördela spänningar till fullo och bärförmågan kan ökas väsentligt jämfört med ett konventionellt limförband.

Contents

Chapter 1

Introduction

1.1 Background

A new type of glued joint is under development, based on the idea of using a rubber foil in the joint to increase the load bearing capacity. The capacity of a traditionally glued joint is limited by concentration of stresses and its low fracture energy which gave rise to the idea of using a rubber foil. Since rubber has the ability to distribute stresses, the capacity of a glued joint is expected to increase substantially using a $0.5-2.0$ mm thick rubber foil between the two adhesive layers. The principal design of a glued rubber foil joint can be seen in Figure 1.1. [6]

Figure 1.1: *Principal design of a glued joint with a rubber foil.*

1.2 Purpose

The purpose of this study is to examine the possibilities of glued rubber foil timber joints. The capacity is limited by failure as well as keeping deformations within an acceptable range. Furthermore, the work comprises a parameter study in order to evaluate the influence of specific parameters on the load bearing capacity for a chosen type of joint.

1.3 Formulation of the task

The study comprises strength and deformation analyses of glued rubber foil timber joints by experimental tests and finite element analyses. The strength and deformation analyses relate to both short term ramp loading and long duration of constant load.

Rubber has a complex mechanical behaviour. The material is characterized by a nonlinear stress-strain relationship which also shows a significant time dependency. It is of great importance to model these properties correctly in order to achieve reliable results from the finite element analyses. Thus, the development of a material model has to be done very carefully.

The main joint type chosen to be studied in application calculations was glued in rods for timber structures, see Figure 1.2. Since the rubber can be vulcanised directly to the steel rod, the rods can be produced and delivered with the rubber foil to the work site ready to be glued in. The analyses of the glued in rods include a parameter study and a study of the time dependency of the load bearing capacity. In the parameter study, the influence of the glued in length on the short term load bearing capacity is evaluated.

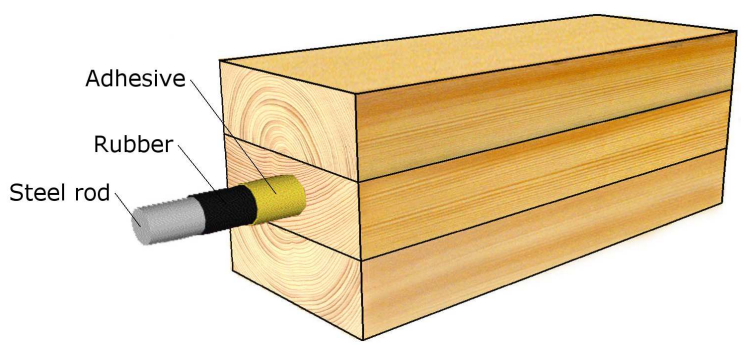

Figure 1.2: *Main joint type of Master's dissertation.*

1.4 Procedure of solving the task

The experimental tests analysed in this study consists of both previously performed tests and tests performed as a part of this study. ABAQUS 6.5 is used for finite element analyses and MATLAB is used for other numerical calculations as well as for plotting test- and calculation results.

The following procedure was used in the work of solving the task:

1. Execution of experimental tests.
2. Compilation and analysis of experimental test results.
3. Development of a preliminary material model for the nonlinear stress vs. strain relationship by analyses of experimental test results.
4. Development of a preliminary material model for the time-dependency of the stress vs. strain relationship by analyses of experimental test results.
5. Calibration and verification of the material models by comparison between experimental test results and results of finite element analyses.
6. Performance of finite element analyses of glued in rods with rubber foil for short- and long term loading in order to investigate the strength and the ability of the rubber foil to distribute the stresses.

Chapter 2

Theory

2.1 Mechanical properties of rubber

Rubber is a polymeric material which becomes elastic by vulcanisation. In the vulcanisation process the long molecular chains are linked together and a solid material with elastic properties is formed. To increase the stiffness of the rubber, different fillers are added before the vulcanisation, such as carbon black. The stiffness of the rubber is described by the hardness-number, which is measured in degrees Shore A or IRHD (international rubber hardness degrees) in a scale of 0-100. [1]

The most advantageous properties of rubber in engineering applications are the ability to remain elastic up to high strain values, the dynamic damping property, the resistance to wear and the relatively high fracture energy. The stiffness of the rubber depends on the amount of fillers being used; increased amount of filler giving a harder and less compliant rubber. The long molecular chains and their ability to stretch and orient themselves in the strain direction explain the elastic behaviour. Strains of several hundred percent are possible to reach. [1]

Rubber is often modelled as a *hyperelastic* material. The stress vs. strain performance of rubber is elastic and more or less nonlinear with a first convex part followed by a concave part [3]. This behaviour is illustrated in Figure 2.1. Different deformation modes of rubber have different straining behaviour with increasing stress. Simple shear shows a more linear relationship between stress and strain than the case of compression or tension. For moderate strains, the shear modulus G can almost be considered a material constant. In the case of large strains, both the tangential shear stiffness and normal stiffness vary with the magnitude of the strain. [1]

Rubber is also distinguished by its nearly *incompressible* properties, which means that it cannot change volume. The shear stiffness is very low compared to the volumetric stiffness. A typical rubber for engineering applications has a bulk modulus (volumetric stiffness) of $1000 - 2000$ MPa and a shear modulus of about 1 MPa. The compressibility of a material is described by Poisson's ratio, ν, which is the ratio between the strains perpendicular and parallel to the direction of the load. Poisson's ratio for rubber is very close to 0.5. [4]

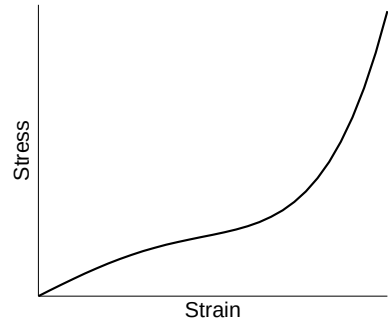

Figure 2.1: *Typical behaviour of a hyperelastic rubber material.*

For long-term loading, rubber shows a nonlinear creep behaviour. This time-dependent viscous effect is called *viscoelasticity* and is an important material property that has to be taken into account when modelling rubber. [6]

2.1.1 Hyperelastic properties

A hyperelastic material is defined as a material whose stresses can be defined by a strain energy function. The constitutive law for a hyperelastic material is defined as a relationship between total stress and total strain where the stresses are determined by derivatives of the strain energy function. Before going into establishing expressions for the strain energy function some terms need to be defined and explained. If nothing else is stated, the theory in this subsection is from [2].

Stretch λ

Instead of the traditionally used strain measure ϵ, defined as the ratio between elongation (relative displacement) Δu and original length L, the strain can be expressed in terms of *stretch* λ. Stretch is defined as the ratio between deformed length l and undeformed length L and is a suitable strain measure for large strain problems.

$$\epsilon = \Delta u / L \tag{2.1}$$
$$\lambda = l/L = 1 + \epsilon \tag{2.2}$$

Deformation gradient $\mathbf{F}$

Consider a 3D-body in a fixed Cartesian coordinate system as in Figure 2.2. The position of a material point in the undeformed body is denoted $\mathbf{X}$, the position of the same material point in the deformed body is denoted $\mathbf{x}$ and the distance between the two points (displacement) is denoted $\mathbf{u}$. The deformation can be expressed as a mapping of the undeformed body into the deformed body according to:

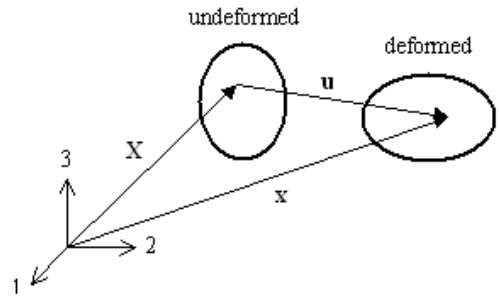

Figure 2.2: *3D body in a cartesian coordinate system.*

$$\mathbf{x} = \mathbf{X} + \mathbf{u} \tag{2.3}$$

$$\mathbf{x} = \mathbf{x}(\mathbf{X}) \tag{2.4}$$

$$\begin{bmatrix} x_1 \\ x_2 \\ x_3 \end{bmatrix} = \begin{bmatrix} x_1(X_1, X_2, X_3) \\ x_2(X_1, X_2, X_3) \\ x_3(X_1, X_2, X_3) \end{bmatrix} \tag{2.5}$$

Differentiation of Equation 2.5 yields the following expression (explicit and in compact form), describing the relationship between a deformed and undeformed infinitesimal line of the body, concerning length and direction:

$$\begin{bmatrix} dx_1 \\ dx_2 \\ dx_3 \end{bmatrix} = \begin{bmatrix} \frac{\partial x_1}{\partial X_1} & \frac{\partial x_1}{\partial X_2} & \frac{\partial x_1}{\partial X_3} \\ \frac{\partial x_2}{\partial X_1} & \frac{\partial x_2}{\partial X_2} & \frac{\partial x_2}{\partial X_3} \\ \frac{\partial x_3}{\partial X_1} & \frac{\partial x_3}{\partial X_2} & \frac{\partial x_3}{\partial X_3} \end{bmatrix} \begin{bmatrix} dX_1 \\ dX_2 \\ dX_3 \end{bmatrix} \tag{2.6}$$

$$\mathbf{dx} = \mathbf{FdX} \tag{2.7}$$

The matrix $\mathbf{F}$ is called the *deformation gradient*. The deformation gradient is however dependent on rigid body motion which makes it unsuitable as a strain measure since rigid body motion does not give rise to stresses and strains in a body. By multiplying the deformation gradient $\mathbf{F}$ with its transpose, the left Cauchy-Green deformation tensor $\mathbf{B}$ is obtained:

$$\mathbf{B} = \mathbf{F}\mathbf{F}^{\mathbf{T}} \tag{2.8}$$

This tensor has the sought property of being independent of rigid body motion and can therefore be used as a strain measure since it carries all necessary information about the deformation.

Strain energy function

The strain energy function W is expressed as strain energy per undeformed unit volume and can be determined from the left Cauchy-Green deformation tensor **B**:

$$W = W(\mathbf{B}) \tag{2.9}$$

Since the state of deformation is fully described by the principal stretches and the principal directions, the strain energy function can be written as:

$$W = W(\lambda_1, \lambda_2, \lambda_3, \mathbf{n}_1, \mathbf{n}_2, \mathbf{n}_3) \tag{2.10}$$

Where λ_i are the principal stretches and $\mathbf{n}_i$ are the principal directions. Since rubber can be considered an isotropic material, the principal directions can thus be ignored and the strain energy function is only dependent on the stretches according to:

$$W = W(\lambda_1, \lambda_2, \lambda_3) \tag{2.11}$$

The strain invariants I_i can be used instead of the stretches λ_i to express the strain energy potential. The strain invariants are other measures for the state of deformation which can be derived from the left Cauchy Green deformation tensor **B** and be expressed in terms of the principal stretches according to:

$$W = W(I_1, I_2, I_3) \tag{2.12}$$
$$I_1 = tr(\mathbf{B}) = \lambda_1^2 + \lambda_2^2 + \lambda_3^2 \tag{2.13}$$
$$I_2 = \frac{1}{2}\left[(tr\mathbf{B})^2 - tr(\mathbf{B}^2)\right] = \lambda_1^2\lambda_2^2 + \lambda_1^2\lambda_3^2 + \lambda_2^2\lambda_3^2 \tag{2.14}$$
$$I_3 = det(\mathbf{B}) = \lambda_1^2\lambda_2^2\lambda_3^2 \tag{2.15}$$

However, the third strain invariant I_3 describes the change in volume and can, due to the nearly incompressible behaviour, be assumed to be equal to 1. This assumption means that I_3 can be used to express λ_3 in terms of λ_1 and λ_2 which results in the following expression for the strain energy function:

$$W = W(I_1, I_2) \tag{2.16}$$
$$I_1 = \lambda_1^2 + \lambda_2^2 + \frac{1}{\lambda_1^2\lambda_2^2} \tag{2.17}$$
$$I_2 = \lambda_1^2\lambda_2^2 + \frac{1}{\lambda_1^2} + \frac{1}{\lambda_2^2} \tag{2.18}$$

By the use of the energy principle (external work equal to total strain energy) the constitutive law for a *hyperelastic*, *isotropic* and *incompressible* material is given by:

$$\boldsymbol{\sigma} = 2(\frac{\partial W}{\partial I_1} + I_1\frac{\partial W}{\partial I_2})\mathbf{B} - 2\frac{\partial W}{\partial I_2}\mathbf{B}^2 + p\mathbf{1} \tag{2.19}$$

where p is the pressure stress and $\mathbf{1}$ is the identity matrix. The derivation is not carried out here but can be found in [8]. The parameters describing the hyperelastic behaviour of a specific material are included in the derivatives of the strain energy function, $\frac{\partial W}{\partial I_i}$, as will be shown later in this chapter.

Simple shear

The deformation mode known as simple shear is illustrated in Figure 2.3 below.

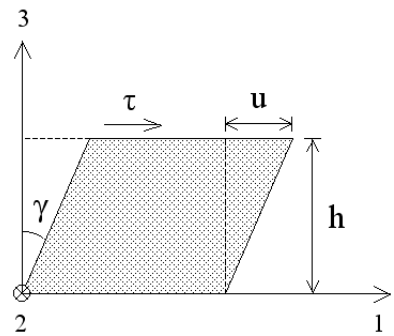

Figure 2.3: *Deformation mode simple shear.*

The relationship between stress and strain for an elastic body in small strain simple shear is well known:

$$\tau = \gamma G \tag{2.20}$$

where the angle γ is used as measure for the shear strain and G the shear modulus. For the case of large deformations the shear strain measure κ is often used:

$$\tau = \kappa G \tag{2.21}$$
$$\kappa = u/h = \tan\gamma \tag{2.22}$$

The height h is constant and normal stresses may be present in all directions. The deformation gradient $\mathbf{F}$, left Cauchy Green deformation tensor $\mathbf{B}$ and the strain invariants I_1 and I_2 for a body in simple shear are given by:

$$\mathbf{F} = \begin{bmatrix} 1 & 0 & \kappa \\ 0 & 1 & 0 \\ 0 & 0 & 1 \end{bmatrix} \tag{2.23}$$

$$\mathbf{B} = \mathbf{F}\mathbf{F}^{\mathbf{T}} = \begin{bmatrix} 1+\kappa^2 & 0 & \kappa \\ 0 & 1 & 0 \\ \kappa & 0 & 1 \end{bmatrix} \tag{2.24}$$

$$\mathbf{B}^2 = \begin{bmatrix} 1+3\kappa^2+\kappa^4 & 0 & 2\kappa+\kappa^3 \\ 0 & 1 & 0 \\ 2\kappa+\kappa^3 & 0 & 1+\kappa^2 \end{bmatrix} \tag{2.25}$$

$$I_1 = tr(\mathbf{B}) = 1+\kappa^2+1+1 = 3+\kappa^2 \tag{2.26}$$

$$I_2 = \frac{1}{2}\left[(tr\mathbf{B})^2 - tr(\mathbf{B}^2)\right] = \\ = \frac{1}{2}\left[(3+\kappa^2)^2 - (1+3\kappa^2+\kappa^4+1+1+\kappa^2)\right] = 3+\kappa^2 \tag{2.27}$$

Using Equation 2.19 and the expression for the strain invariants given above results in the following expression for the stress-strain relationship for a body in simple shear [1]:

$$\begin{bmatrix} \sigma_{11} & \sigma_{12} & \sigma_{13} \\ \sigma_{21} & \sigma_{22} & \sigma_{23} \\ \sigma_{31} & \sigma_{32} & \sigma_{33} \end{bmatrix} = 2\left(\frac{\partial W}{\partial I_1} + (3+\kappa^2)\frac{\partial W}{\partial I_2}\right) \begin{bmatrix} 1+\kappa^2 & 0 & \kappa \\ 0 & 1 & 0 \\ \kappa & 0 & 1 \end{bmatrix} \\ -2\frac{\partial W}{\partial I_2} \begin{bmatrix} 1+3\kappa^2+\kappa^4 & 0 & 2\kappa+\kappa^3 \\ 0 & 1 & 0 \\ 2\kappa+\kappa^3 & 0 & 1+\kappa^2 \end{bmatrix} + p \begin{bmatrix} 1 & 0 & 0 \\ 0 & 1 & 0 \\ 0 & 0 & 1 \end{bmatrix} \tag{2.28}$$

Since the only shear stress components different from zero are σ_{13} and σ_{31}, the shear stress τ is given by:

$$\tau = \sigma_{13} = \sigma_{31} = 2\left(\frac{\partial W}{\partial I_1} + \frac{\partial W}{\partial I_2}\right)\kappa \tag{2.29}$$

2.1.2 Hyperelastic material models

There are several different material models available for modelling hyperelasticity in rubber. There is not one model that is better than the others for all applications and the choice of model needs to be made on basis of a variety of factors. These factors include type of rubber (natural rubber, carbon-black-filled rubber etc), type of application (level of stresses and strains, deformation mode etc) and also availability of test data (uniaxial, biaxial, pure shear, simple shear etc). [1]

Many of these hyperelastic material models are based on the polynomial form of the strain energy function W. The general form of the polynomial strain energy function is given by the series expansion according to [1]:

$$W = \sum_{i=0}^{\infty}\sum_{j=0}^{\infty} C_{ij}(I_1 - 3)^i(I_2 - 3)^j \tag{2.30}$$

The specific behaviour of a material is defined by the constants C_{ij}. This general expression can be altered by using a limited number of terms or by excluding certain terms in the series. Fairly simple models, which may well describe the behaviour of a certain rubber, can be obtained in this way. The first term, C_{00}, is always excluded since the strain energy function is required to be zero at an undeformed state. A short description of two hyperelastic material models is presented below.

Neo Hooke

Using only the first term in the series gives the Neo Hooke material model [2].

$$\begin{aligned} W &= C_{10}(I_1 - 3) && (2.31)\\ \frac{\partial W}{\partial I_1} &= C_{10} && (2.32)\\ \frac{\partial W}{\partial I_2} &= 0 && (2.33)\\ \tau &= 2(\frac{\partial W}{\partial I_1} + \frac{\partial W}{\partial I_2})\kappa = 2C_{10}\kappa && (2.34) \end{aligned}$$

The Neo Hooke model can often give satisfactory results when fitted to test data for simple shear at low strain levels because of the almost linear relationship between stresses and strains for this deformation mode. If the stress-strain relationship behaves in a highly nonlinear manner, this model will only be accurate at certain intervals. [2]

Yeoh

The Yeoh-model is obtained by excluding all terms including the second strain invariant I_2 and using only terms corresponding to $i = 1, 2, 3$ and $j = 0$ in the general polynomial expression [2].

$$\begin{aligned} W &= C_{10}(I_1 - 3) + C_{20}(I_1 - 3)^2 + C_{30}(I_1 - 3)^3 && (2.35)\\ \frac{\partial W}{\partial I_1} &= C_{10} + 2C_{20}(I_1 - 3) + 3C_{30}(I_1 - 3)^2 && (2.36)\\ \frac{\partial W}{\partial I_2} &= 0 && (2.37)\\ \tau &= 2(\frac{\partial W}{\partial I_1} + \frac{\partial W}{\partial I_2})\kappa = 2C_{10}\kappa + 4C_{20}\kappa^3 + 6C_{30}\kappa^5 && (2.38) \end{aligned}$$

The reason for excluding the terms including I_2 is that the dependence on the second strain invariant is weak in comparison to the first invariant. It has been shown that this model describes the behaviour for carbon-filled rubbers rather well [2].

2.1.3 Viscoelastic properties

The theory of this Subsection is from [2].

Viscoelastic properties include creep (time dependent increase of strains under constant stress) and relaxation (time dependent decrease of stresses under constant strain). The relaxation or creep of a viscoelastic material can be described by the use of rheological models with springs and dashpots according to Figure 2.4. By connecting these two elements using parallel and series connections, more advanced rheological models can be obtained. Connecting a spring in series with a dashpot yields the Maxwell model. By expanding the Maxwell model with a parallel spring, the Zener model is obtained. A model which can accurately describe the properties of a viscoelastic material is the generalised Maxwell model. This model consists of a Zener model with not just one but a number N of Maxwell models parallel to a spring, see Figure 2.5.

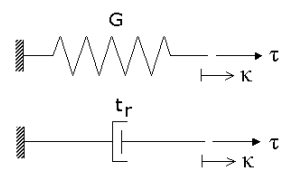

Figure 2.4: *Spring element (top) and dashpot element (bottom).*

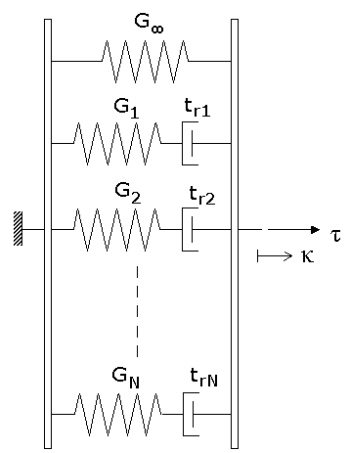

Figure 2.5: *Generalised Maxwell model.*

The generalised Maxwell model can be used to describe a time-varying stiffness $G(t)$ with specified values for G_∞, G_i and t_{ri} according to:

$$G(t) = G_\infty + \sum_{i=1}^{N} G_i \cdot e^{-t/t_{ri}} \tag{2.39}$$

$$G(0) = G_0 = G_\infty + \sum_{i=1}^{N} G_i \tag{2.40}$$

$$G(\infty) = G_\infty \tag{2.41}$$

At a time $t = 0$, the total stiffness of the system is the sum of the stiffness of all connected springs. As time increases, the dashpots will be relaxed according to their individual relaxation times t_{ri} and the total stiffness $G(t)$ of the system will decrease. Finally, at a time $t = \infty$, the stiffness of the model will only be dependent upon the stiffness of the spring denoted G_∞.

It can many times be useful to describe the decreasing stiffness over time as a *dimensionless* relaxation modulus $g_R(t)$, where R stands for relaxation. The dimensionless relaxation modulus $g_R(t)$ is defined by a set of prony coefficients g_i and corresponding relaxation times t_{ri}. The prony coefficients are obtained by dividing the stiffness of the individual springs G_i with the initial stiffness G_0 of the whole system according to Equation 2.44. The sum of the prony coefficients g_i corresponds to the loss of stiffness at $t = \infty$ and must be < 1. The dimensionless relaxation modulus (Equation 2.44) is obtained by dividing $G(t)$ with G_0 according to:

$$G(t) = G_\infty + \sum_{i=1}^{N} G_i e^{-t/t_{ri}} = G_0 - \sum_{i=1}^{N} G_i (1 - e^{-t/t_{ri}}) \tag{2.42}$$

$$g_i = \frac{G_i}{G_0} \tag{2.43}$$

$$g_R(t) = 1 - \sum_{i=1}^{N} g_i (1 - e^{-t/t_{ri}}) \tag{2.44}$$

Figure 2.6 shows an example of possible relaxation modulus $g_R(t)$ with $N = 3$.

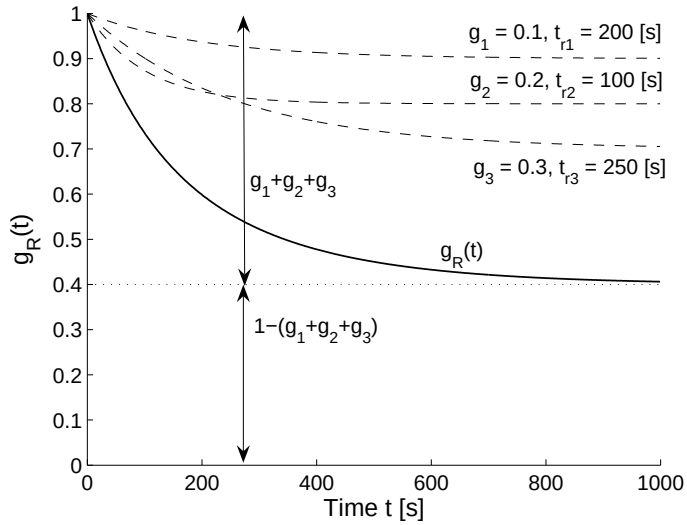

Figure 2.6: *Example of dimensionless relaxation modulus $g_R(t)$.*

2.2 FE-modelling of rubber in ABAQUS

2.2.1 Hyperelastic materials

When modelling a hyperelastic material in ABAQUS, the program makes the following assumptions [4]:

- The material behaviour is elastic.
- The material behaviour is isotropic.
- The simulation will include non-linear geometric effects.

Elastomeric materials are initially assumed to have random orientations of the long-chain molecules. When the material is stretched, the structure of the molecules is changed and anisotropy develops. The assumption of isotropy even after deformation is made considering that the development of this anisotropy follows the direction of straining. [4]

Hybrid elements

For the choice of element type for a hyperelastic material in ABAQUS, *hybrid* elements are recommended. These elements are also called *mixed formulation* elements since a mixture of displacement and stress variables are used to approximate the equilibrium equations and compatibility conditions. Volumetric strain locking can

occur if the finite element mesh cannot properly represent the deformations of incompressible materials. By use of hybrid elements, the risk of volumetric strain locking is avoided. [7]

Specification of hyperelastic properties

In ABAQUS, the material properties of a hyperelastic material can be defined by test data from experimental stress vs. strain tests. Four different kinds of tests can be used at the same time to get an accurate approximation of the material parameters. These tests are uniaxial, planar (pure shear test), equibiaxial and volumetric tests. Another way of describing the material behaviour is by direct specification of coefficients for the chosen hyperelastic material model. [4]

2.2.2 Viscoelastic materials

The relaxation of a material is computed in ABAQUS by decreasing the stiffness over time according to specified data. This is done, according to Equation 2.45, by applying the dimensionless relaxations modulus $g_R(t)$ on the coefficients C_{ij} that define the strain energy function according to Equation 2.30. For a material subjected to creep or a varying load history, the strains are integrated over time.

$$C_{ij}^R(t) = C_{ij}^0 \cdot g_R(t) = C_{ij}^0 \cdot [1 - \sum_{i=1}^{N} g_i(1 - e^{-t/t_{ri}})] \tag{2.45}$$

Specification of viscoelastic properties

The viscoelastic behaviour of a material can be defined in four separate ways [4]:

- Direct specification of the prony coefficients g_i.
- Inclusion of creep test data.
- Inclusion of relaxation test data.
- Inclusion of frequency dependent data from sinusoidal oscillation experiments.

2.2.3 Creep behaviour of Neo Hooke and Yeoh models

As mentioned above, ABAQUS computes decreasing stiffness under constant load by applying the dimensionless relaxation modulus $g_R(t)$ on the Yeoh coefficients C_{10}, C_{20} and C_{30} according to Equation 2.45. In order to exemplify this, imagine a hypothetic rubber material with the following Yeoh coefficients describing the initial hyperelastic behaviour:

$$\begin{aligned} C_{10} &= 0.3\,\text{MPa} \\ C_{20} &= -0.03\,\text{MPa} \\ C_{30} &= 0.003\,\text{MPa} \end{aligned}$$

The initial stress-strain curve corresponding to these coefficients is represented by the solid line in Figure 2.7. The dimensionless relaxation modulus $g_R(t)$ varies from 1.0 at $t = t_0$ and decreases as time increases. Assume a time $t = t_1$ where $g_R(t_1) = 0.9$ and a constant load. According to Equation 2.45, the Yeoh coefficients are each individually decreased with 10 %, which results in the dashed curve in Figure 2.7. A Neo Hooke material with the same initial shear stiffness ($C_{10} = 0.3$) is also plotted in Figure 2.7.

To illustrate the influence of the stress level on the creep strains, imagine that two creep tests are carried out for a rubber that can be characterised as described above, one at a constant stress level of $\tau = 0.6$ MPa and the other at a constant stress level of $\tau = 2.0$ MPa. Figure 2.8 shows the Yeoh model for $t = t_0 = 0$ and $t = t_1 > 0$ for the two different stress levels.

Both the absolute and the relative creep strains are much larger at $t = t_1$ for the lower stress level compared to the creep strains of the higher stress level for the Yeoh material model, see Table 2.1. This is a consequence of the fact that the creep behaviour is dependent on the tangential stiffness at the current stress level. For the Neo Hooke model, the relative creep strains are the same for the two stress levels.

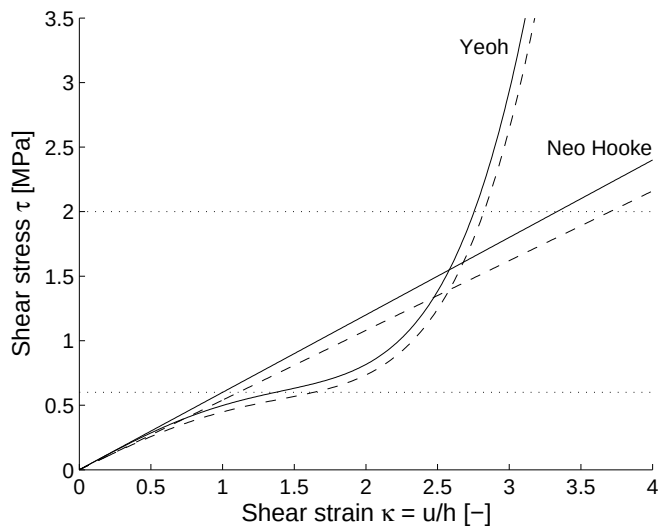

Figure 2.7: *Yeoh and Neo Hooke material models at t_0 and t_1.*

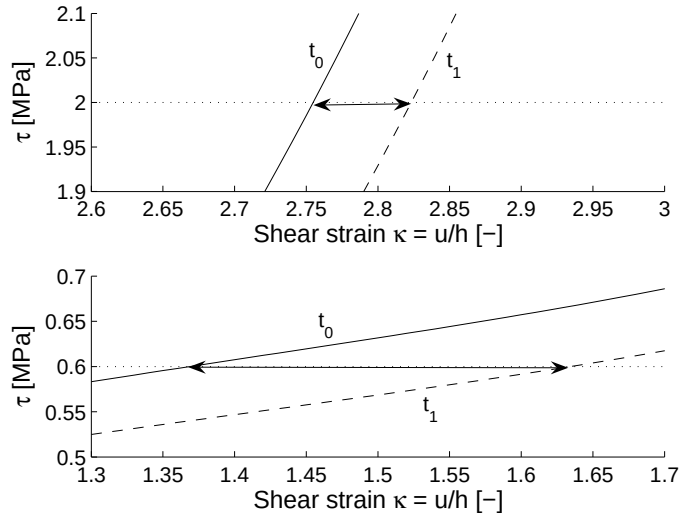

Figure 2.8: *Yeoh material model at $\tau = 2.0$ MPa and $\tau = 0.6$ MPa.*

$$\text{Creep strain} = \kappa(t_1) - \kappa(0) \tag{2.46}$$

$$\text{Relative creep strain} = \text{Creep strain}/\kappa(0) \tag{2.47}$$

Table 2.1: *Shear strains for hypothetic Neo Hooke and Yeoh materials.*

Shear strain		Neo Hooke $\tau = 0.6$ MPa	Neo Hooke $\tau = 2.0$ MPa	Yeoh $\tau = 0.6$ MPa	Yeoh $\tau = 2.0$ MPa
$\kappa(0)$	[-]	1.000	3.333	1.368	2.755
$\kappa(t_1)$	[-]	1.111	3.704	1.634	2.825
Creep strain	[-]	0.111	0.371	0.26	0.07
Rel. creep strain	[%]	11	11	19	2.5

ABAQUS analyses of creep with Neo Hooke and Yeoh models

To further investigate how ABAQUS calculates the creep deformation for the Neo Hooke and the Yeoh models a one-element model of each material was created. The single element was subjected to a uniform shear stress and left to creep under constant shear stress. The shear strains were compared between the two different material models at the two different shear stress levels used above, $\tau = 0.6$ MPa and $\tau = 2.0$ MPa. A set of prony coefficients were used to describe the creep behaviour, see Table 2.2.

Table 2.2: *Used prony coefficients.*

	$g_i\,[-]$	$t_{ri}\,[s]$
i=1	0.05040	10^3
i=2	0.03709	10^4
i=3	0.01335	$2 \cdot 10^5$
i=4	0.02708	10^6
$\sum_{i=1}^{4}$	0.12792	-

The analyses were run for a loading time period of 10^6 seconds ($\approx$ 11.5 days). The results for the first 10 hours can be seen in Figure 2.9 and the results for the whole time period are presented in Table 2.3.

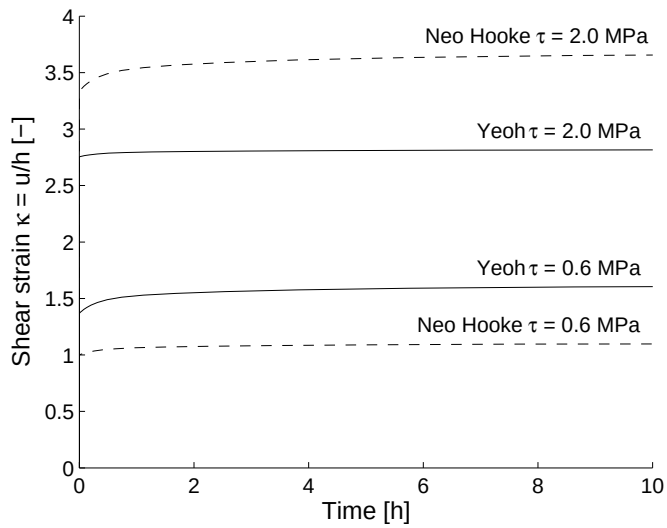

Figure 2.9: *Creep deformation for Neo Hooke and Yeoh material models at different stress levels for the first 10 hours.*

Table 2.3: *Results of FE-analysis for Neo Hooke and Yeoh material models.*

Shear strain		Neo Hooke $\tau = 0.6$ MPa	Neo Hooke $\tau = 2.0$ MPa	Yeoh $\tau = 0.6$ MPa	Yeoh $\tau = 2.0$ MPa
$\kappa(0)$	[-]	1.000	3.333	1.368	2.755
$\kappa(t = 10^6)$	[-]	1.133	3.774	1.680	2.836
Creep strain	[-]	0.133	0.441	0.312	0.0811
Rel. creep strain	[%]	13	13	23	3

From the results of the ABAQUS analyses presented in Figure 2.9 and Table 2.3, it can be seen that the absolute creep deformation for the Neo Hooke material is larger for the higher stress level compared to the lower but the relative creep deformations at the two different stress levels are the same. For the Yeoh material, a higher stress level results in lower creep deformations both in absolute and relative measures, as expected. This conclusion implies that unrealistic creep deformations is generated when using the Yeoh model in combination with viscoelastic properties.

2.2.4 Method for using the Yeoh model in creep calculations

The same prony coefficients describing the viscoelastic response give different results when used with the Yeoh model compared to the Neo Hooke model as described in Subsection 2.2.3. In order to get approximately the same creep behaviour for the two models, a structured method of modifying the prony coefficients g_i was developed.

The magnitude of the creep deformations at a given time is determined by, apart from the stresses, the tangential stiffness of the hyperelastic stress-strain relationship and the value of the relaxation modulus at that time. A low value of the tangential stiffness indicates a softer material that yields larger creep deformations than a high value. The linear Neo Hooke model has a constant tangential stiffness and at a place where the Yeoh model has the same tangential stiffness, use of the same set of prony coefficients should result in the same creep deformations.

A factor $k(\tau)$ is introduced to describe how much the prony coefficients should be increased or decreased in order to yield the same creep deformations for the Neo Hooke and the Yeoh models. The factor k is defined according to Equation 2.48 and the modified prony coefficients for a Yeoh material model are determined according to Equation 2.49.

$$k(\tau) = \frac{(d\tau/d\kappa)_{Yeoh}}{(d\tau/d\kappa)_{NeoHooke}} \tag{2.48}$$

$$g_{i,Yeoh} = k(\tau) \cdot g_{i,NeoHooke} \tag{2.49}$$

The factor $k(\tau)$ can be plotted (for a specific Neo Hooke material and a specific Yeoh material) as a function of shear stress independent of the prony coefficients.

To illustrate this idea, an example is presented with the same two hyperelastic material models as in Subsection 2.2.3. As can be seen in Figure 2.10, the two models yield the same strains at a stress level of approximately 1.5 MPa. Since there is a rather large difference in tangential stiffness between the two models, creep behaviour for a specific set of prony coefficients g_i will be very different although the initial strains will be the same.

The factor $k(\tau)$ can be computed from the known hyperelastic models by first finding the derivative of the stress-strain relationship and then applying Equation 2.48 and Equation 2.49. The derivatives (tangential stiffness) of the two material models and $k(\tau)$ can be seen in Figure 2.11 and Figure 2.12 respectively.

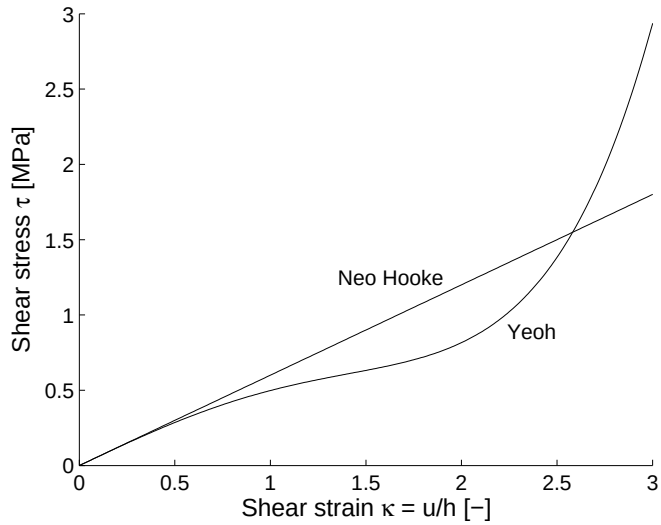

Figure 2.10: *Hypothetic hyperelastic models.*

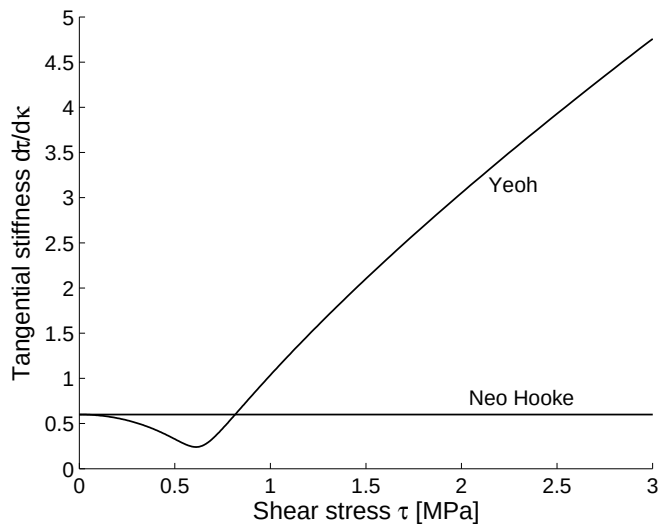

Figure 2.11: *Tangential stiffness $d\tau/d\kappa$ of the hyperelastic models in the example.*

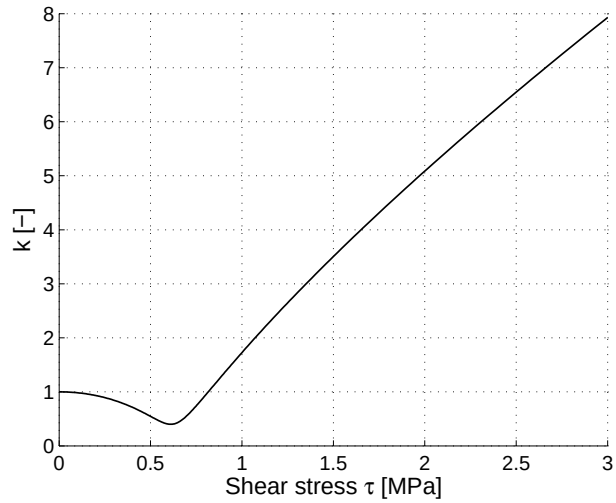

Figure 2.12: *Factor k for the Yeoh model in the example.*

2.3 Fracture theory

2.3.1 Failure criteria for rubber

Failure criteria for rubber is a rather unexplored area. For most engineering applications, rubber is not exposed to stresses close to the stress limit and a failure criterion is therefore of less interest. For the applications concerned within this study, a well defined failure criterion for rubber is, however, needed.

A failure criterion can be based either on stresses, strains or fracture energy. For simple shear, the failure criterion may consist of a maximum shear stress or a maximum shear strain. Two different shear strain criteria, κ_c and κ_f, will be defined in this study. The first criterion describes a serviceability limit and the latter describes the ultimate limit.

Serviceability limit state

The criterion in the serviceability limit state is chosen to be defined as the shear strain at the second inflexion point of the stress vs. strain relationship, see Figure 2.13. At this point, the curve changes from a concave to a convex form. In the concave part, the tangential stiffness increases with increasing strain whereas it is decreasing in the convex part. This change, from increasing to decreasing tangential stiffness, can be assumed to inherit from changes in the microstructure which causes initialisation of failure. The shear stress and shear strain in the serviceability limit state are denoted τ_c and κ_c and the instantaneous shear strain κ_e, see Figure 2.13 and Figure 2.14.

Ultimate limit state

The criterion in the ultimate limit state is simply defined as the shear strain at maximum shear stress of the stress vs. strain relationship, see Figure 2.13. The shear stress and shear strain in the ultimate limit state are denoted τ_f and κ_f.

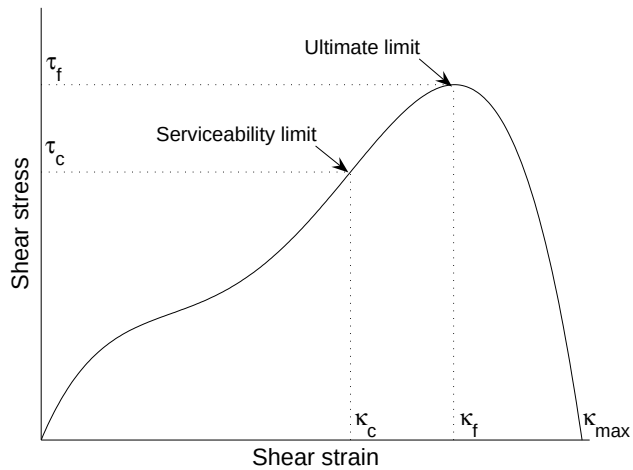

Figure 2.13: *Illustration of criteria for short term ramp loading.*

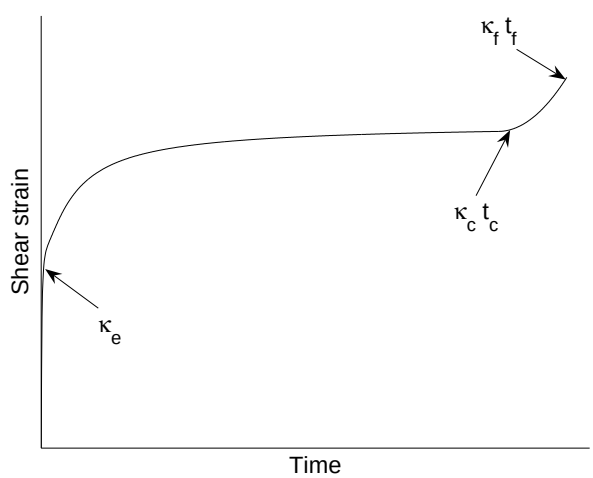

Figure 2.14: *Illustration of criteria for long term constant loading.*

2.3.2 Fracture energy

The fracture energy G_f is defined as the energy absorbed per unit area at failure. The energy W is defined according to Equation 2.50 where P [N] is the applied force, τ the shear stress, A the stressed area [m^2] and h [m] the thickness. This yields the fracture energy G_f according to Equation 2.51.

$$W = \int P\,du = \int_0^{\kappa_{max}} \tau A h\,d\kappa\,[\mathrm{Nm}] \tag{2.50}$$

$$G_f = \frac{W}{A}\,[\mathrm{N/m}] \tag{2.51}$$

Chapter 3

Experimental studies

The experimental studies comprise both previous tests and tests performed within this master's dissertation study. For the previous tests, test data was received and the analyses of the results were performed within this master's thesis.

Previous work

A previous masters thesis, [9], dealing with glued rubber foil joints dealt in particular with the issue of what type of rubber and glue that may be suited for structural use. Several experimental tests were performed in collaboration with the Division of Structural Mechanics at Lund University. Three different types of rubber were examined and reference tests without a rubber foil were also performed within that study. The conclusions were that the most suitable rubber for structural applications would be a mixture of chloroprene rubber (CR) and styrene-butadiene rubber (SBR) and the most suitable glue emulsion-polymere with isocyanate hardener (EPI). These conclusions were established by analysing test data as well as taking other important aspects of the different rubbers (weather resistance, cost etc) into account.

The mechanical tests included a short term ramp loading stress vs. strain test in simple shear. The aim for this test was to determine the hyperelastic behaviour of the different rubbers. This test will be referred to as test MWA in this report. Furthermore, the tests included full scale tests of beams in bending, which will be referred to as test MWF. Only the tests that are used in the development of the material models will be presented and evaluated in this report.

Previous work also contains preliminary long duration of load tests, performed by the staff at the Division of Structural Mechanics at Lund University. The main purpose of these tests was to measure the time to failure at constant load and to study the types of failure.

Materials

The materials used in the experimental studies are presented in Table 3.1.

Table 3.1: *Used materials in experimental studies.*

Material	Quality
Wood	Swedish fir, LT 40
Glue	EPI (Emulsion Polymer Isocyanate) Casco 1984 with hardener 1993
Rubber [10]	CR/SBR (Chloroprene/Styrene-butadien) Trelleborg AB Product nbr. 3932 Shore A = 60 ($\pm$5) NOTE: This rubber is denoted CR in this report

3.1 Stress vs. strain

These tests were carried out in order to examine the hyperelastic behaviour in simple shear by registration of the stress-strain relationship.

3.1.1 Method

The geometry of the test specimens and the attachment device are shown in Figure 3.1 and Figure 3.2. The deformation u was recorded as the relative movement of the pistons to which the specimen was attached. The shear strain was calculated according to $\kappa = u/h$ where h is the thickness of the rubber foil.

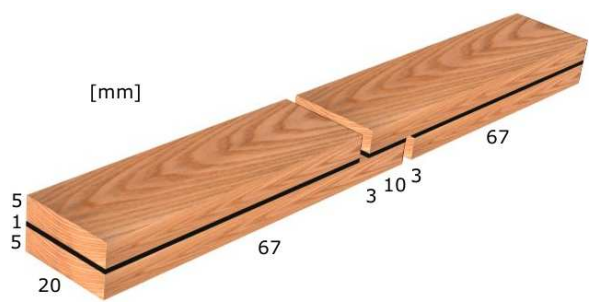

Figure 3.1: *Geometry of test specimen.*

Figure 3.2: *Specimen and attachment device of test MWA.*

3.1.2 Results

Five nominally equal tests were carried out, denoted CR 1, CR 2, CR 3, CR 4 and CR 5. The stress-strain relationships are presented in Figure 3.3 and the strain at serviceability and ultimate limit state, the fracture energy and the failure types are presented in Table 3.2. The fracture energy is determined according to Equation 2.50 and Equation 2.51. The failure types are denoted as r for rubber failure, r-a for failure in the rubber-adhesive interface and w for wood failure.

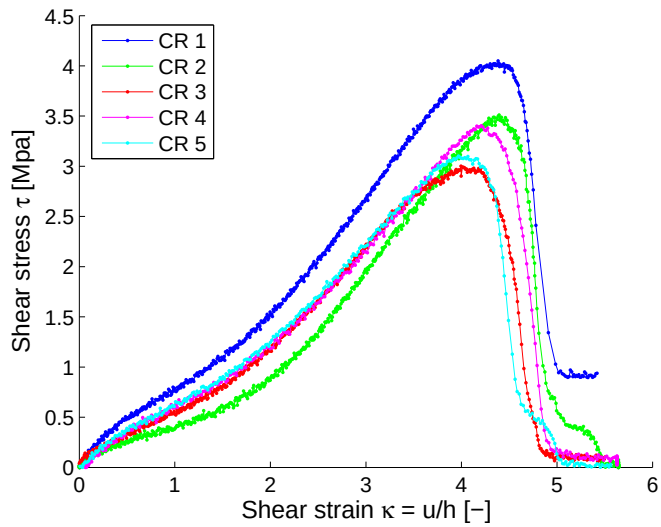

Figure 3.3: *Results of test MWA.*

Table 3.2: *Stress, strain, fracture energy and type of failure for test MWA.*

Spec.nbr	τ_c [MPa]	κ_c [-]	τ_f [MPa]	κ_f [-]	G_f [MN/m]	Type of failure r/r-a/w [%]
CR 1	2.5	2.9	4.049	4.383	0.0106	75/25/0
CR 2	1.9	3.0	3.512	4.394	0.0077	98/2/0
CR 3	1.7	2.5	3.001	3.995	0.0073	80/20/0
CR 4	1.8	2.6	3.405	4.209	0.0080	75/25/0
CR 5	1.8	2.6	3.101	3.969	0.0074	80/20/0
Mean (CR 1-5)	1.94	2.72	3.414	4.190	0.0082	-
Std (CR 1-5)	0.321	0.217	0.443	0.204	0.0014	-
Mean (CR 3-5)	1.77	**2.57**	3.169	**4.058**	0.0076	-
Std (CR 3-5)	0.058	0.058	0.210	0.132	0.0004	-

Establishment of failure criteria

Although the five specimens show significant differences regarding the hyperelastic behaviour, the shear strains at failure are rather equal. The variation of the maximum shear stress for the three tests CR 3, CR 4 and CR 5 are larger than the variation of the corresponding shear strains. This observation suggests that a failure criterion based on strain is more suitable compared to a stress-based criterion. The theory and definitions of the strain criteria for serviceability- and ultimate limit state are presented in Section 2.3.

The established failure criteria for serviceability- and ultimate limit state are based on test CR 3, CR 4 and CR 5 and read:

$$\textit{serviceability limit:} \qquad \kappa_c \approx 2.57 \tag{3.1}$$

$$\textit{ultimate limit:} \qquad \kappa_f \approx 4.06 \tag{3.2}$$

3.1.3 Discussion

As can be seen in Figure 3.3, the test results were somewhat scattered. Two curves show rather large dissimilarities with the three curves gathered in the middle. Since three out of the five specimens show a very similar response it is rather unlikely that the material itself has such a great variation. The reasons for these dissimilarities might instead have been caused by lack of consistency in the test procedure or other problems during the testing or production of the specimens. The three curves in the middle (CR 3, CR 4 and CR 5) were therefore assumed to represent the hyperelastic behaviour well since they show similar responses. The two specimens CR 1 and CR 2 were disregarded in the evaluation of material stiffness parameters. Further evaluation of the results of this test is made in Section 4.1.

3.2 Full-scale bending of beams

Full-scale beams were tested in bending in order to investigate the influence on the load bearing capacity when using a rubber foil in the glued joint.

3.2.1 Method

Six specimens were tested, three with a 1 mm rubber foil and three reference beams with conventionally glued joints. PRF-glue was used for the reference joints while EPI-glue was used for the rubber joints. The joints were let to harden for 10 days and all specimens were conditioned at 60 % RH and 20^{o}C.

The force was applied as a point load acting on a steel profile dividing the one point load into two loads acting on the beam. The deflection was recorded as the stroke of the actuator, acting on the steel profile. The geometry of the specimens is shown in Figure 3.4 and test setup was made according to Figure 3.5.

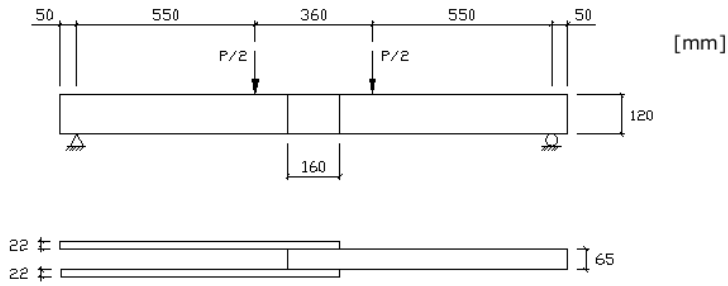

Figure 3.4: *Geometry of full scale beam.*

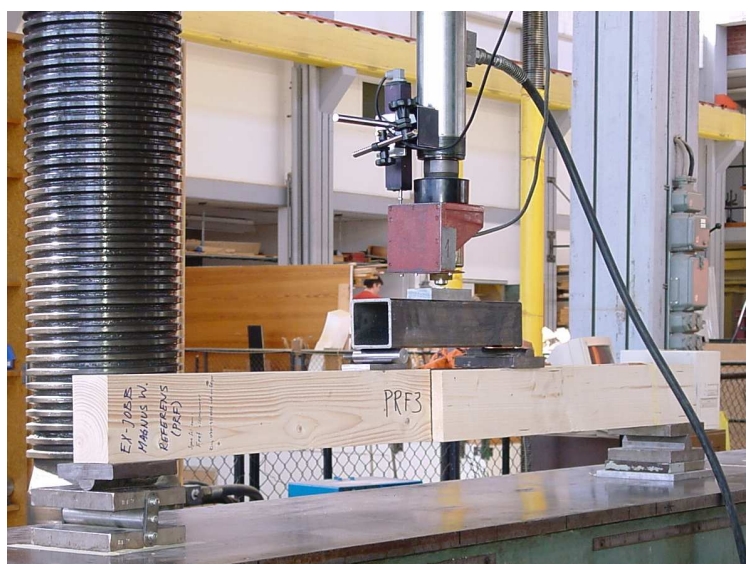

Figure 3.5: *Test setup of full scale test.*

3.2.2 Results

The results of the six tests are presented in Figure 3.6 and Table 3.3. Figure 3.6 shows that for the beams with a rubber foil, failure is initialised at a deflection of 25-30 mm and a load of about 15 kN. The conventionally glued beams show a lower maximum load bearing capacity and smaller deflections compared to the beams with rubber foils. In FCR 2, which gave the lowest load bearing capacity out of the three rubber foil beams, the failure occurred due to bending failure of the wood outside the joint area. The results of FCR 2 are therefore excluded from the mean value calculation shown in Table 3.3.

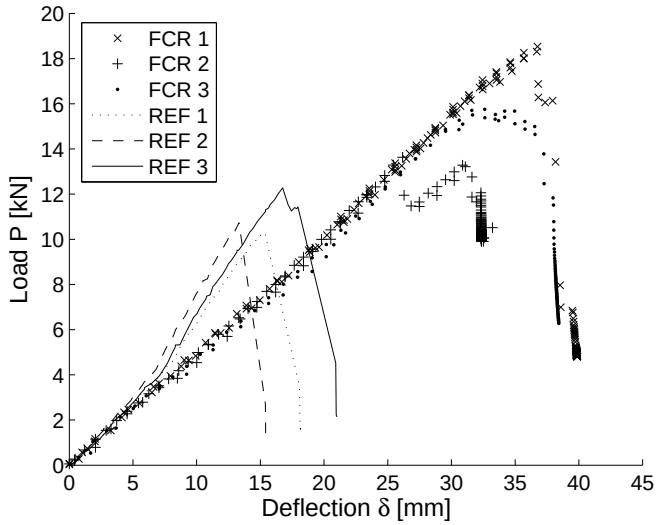

Figure 3.6: *Results of test MWF.*

Table 3.3: *Ultimate load P_{max} and deflection at ultimate load δ_{Pmax}.*

CR-Foil	P_{max} [kN]	δ_{Pmax} [mm]	Reference	P_{max} [kN]	δ_{Pmax} [mm]
FCR 1	18.53	36.75	REF 1	10.31	15.34
(FCR 2	13.63	26.17)	REF 2	10.73	13.32
FCR 3	15.75	32.62	REF 3	12.28	16.75
Mean (FCR 1,3)	17.14	34.68	Mean	11.10	15.14
Std (FCR 1,3)	1.964	2.927	Std	1.037	1.723

3.3 Preliminary long duration of load test

These tests were performed in order to get some preliminary knowledge about the time-dependency of the strength during constant load [6].

3.3.1 Method

The test specimens were of the same geometry as in the stress vs. strain test, see Figure 3.1. A total of eight specimens were loaded at two different load levels, four with approximately 32 kg and the other four with approximately 48 kg, and the times to failure were recorded. In the tests, two different kinds of rubber was used, chloroprene/styrenbutadien rubber (CR) and another, not defined type (X). The setup of this test was the same as the setup for the creep test described in the below Subsection 3.4.1 apart from the gauge used for measuring deformation.

3.3.2 Results

The results of the preliminary long duration of load tests are presented in Table 3.4 and the types of failure can be seen in Figure 3.7. The failure types are denoted as r for rubber failure, r-a for failure in the rubber-adhesive interface and w for wood failure.

Table 3.4: *Time to failure and type of failure for preliminary long duration of load test.*

Spec	Rubber	Load [kg]	τ [MPa]	Time [h]	Type of failure r/r-a/w [%]
A1	X	32.23	1.58	125.42	100/0/0
A2	CR	32.75	1.61	1.61	10/90/0
A3	X	32.66	1.60	126.99	100/0/0
A4	CR	32.52	1.60	87.07	80/10/10
A5	X	48.90	2.40	1.20	90/0/10
A6	CR	48.37	2.37	0.89	75/25/0
A7	X	48.67	2.39	1.36	75/0/25
A8	CR	48.00	2.35	12.34	100/0/0

Figure 3.7: *Failure types of the test specimens.*

3.3.3 Discussion

Specimen A2 collapsed much earlier than the other three with the same load. The failure did not occur within the rubber foil but mainly in the rubber-glue interface which indicates that the gluing was not carried out properly. The specimens with pure rubber-failure lasted the longest time and were clearly strongest. For the specimens with 48 kg load the same tendency can be seen, observing that the specimen with 100 % rubber-failure lasted twelve times longer than the others. These results implies that the gluing is critical and has to be carried out carefully and correctly. This is also verified by the results of the creep test presented later on in this chapter.

3.4 Creep test

The creep test was performed in order to determine the viscoelastic behaviour of the rubber. Another aspect of the test was to study the types of failure and the time to failure as in the preliminary long duration of load test.

3.4.1 Method

The geometry of the test specimens was the same as in the stress vs. strain test, see Figure 3.1. The test was performed in two sets, denoted as test B and test C. In test B, two different levels of loads were used, a lower level with a weight of approximately 32-33 kg and a higher level of approximately 48-49 kg. Test C was performed in order to complement the results of creep test B and study the creep behaviour at a lower stress level. This test consisted of three specimens with a load of 16 kg and one complementary specimen with a load of 32 kg.

The load was applied smoothly by an hydraulic lifting instrument with a duration of about 10 seconds from zero load to full load. For test B, the elongation was recorded once every minute until failure occurred. In the latter test, test C, the measuring of the elongation was made once every 15 seconds for the first 15 minutes and thereafter decreased gradually to once every three hours after 48 hours. This was done after noticing in the results of test B that the creep rate is significantly higher in the beginning of the creep phase as can be seen in Figure 3.10. Since some specimens did not fail during the work of the master's dissertation, the measuring continued for the possible use of the results in future studies. The temperature in the test room was 25 °C and the relative humidity was 30-40 %.

The rubber in the test specimens were of two different types, CR and the unknown type X. The unknown type was tested in hope of the rubber also being CR. If the results were similar between the tests, the rubber marked X could be assumed to be of the same quality as the rubber marked CR. Otherwise the quality would still be unknown and the results would be of less value.

Test setup

The test setup was made with the intention of achieving a deformation state of simple shear with constant and homogeneous shear stress in the rubber foil. The test rig used allowed eight tests to be carried out simultaneously. The specimens were loaded by attaching weights consisting of steel plates with a weight of about 16 kg each. The deformation was measured by attaching a gauge to the upper part of the specimen and a small steel plate to the bottom. Since there were two different ways of attaching the measuring gauges, see Figure 3.14, the respective ways were used on half of the specimens. The measuring gauge used were linear sensors of type 9610 R3.4K L2.0 of the make Duncan with a repeatability within 0.013 mm. The test rig and the individual test setup can be seen in Figure 3.8 and Figure 3.9.

Figure 3.8: *Test rig used for creep tests.*

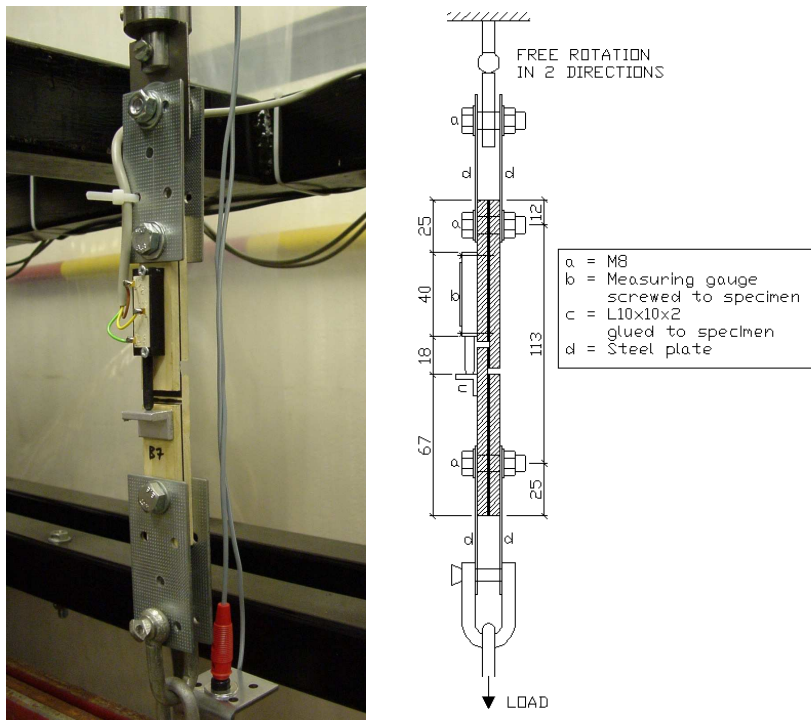

Figure 3.9: *Specimen B7 during testing (left) and sketch of test setup (right).*

3.4.2 Results

Figure 3.10, Figure 3.11 and Figure 3.12 show the recorded deformations for the three load levels of the creep test in different time scales. The results for the specimens with X-rubber showed that the rubber cannot be CR-rubber and are therefore not used in the further work of developing a material model. Hence, only the results of the CR-specimens are presented in the figures. Figure 3.10 shows the sudden increases in deformation that occurred in test B after about 2.5 and 3.5 hours. This problem is discussed in Subsection 3.4.3.

Table 3.5 shows the strain, the time to failure and failure types for all test specimens. In these tests, the instantaneous strain, κ_e, is defined as the strain one minute after the start of the loading. The strain at the serviceability limit, κ_c, and at the ultimate limit, κ_f, are defined in Figure 2.14 for long term loading. In the same manner as in Table 3.4, the failure types are denoted as r for rubber failure, r-a for failure in the rubber-adhesive interface and w for wood failure. The failure types of the test specimens are also presented in Figure 3.13. In order to clarify the comparison between the instantaneous deformation of the creep test and the instantaneous deformation of test MWA at corresponding stress levels, Table 3.6 is provided.

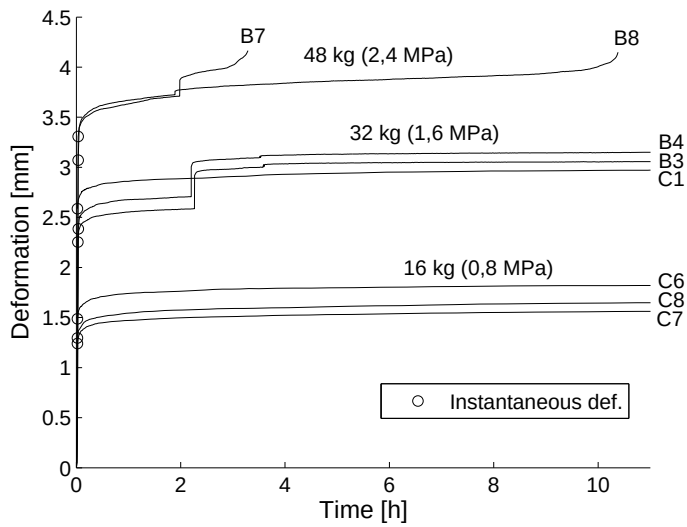

Figure 3.10: *Creep test results of CR rubber, 0-11 h.*

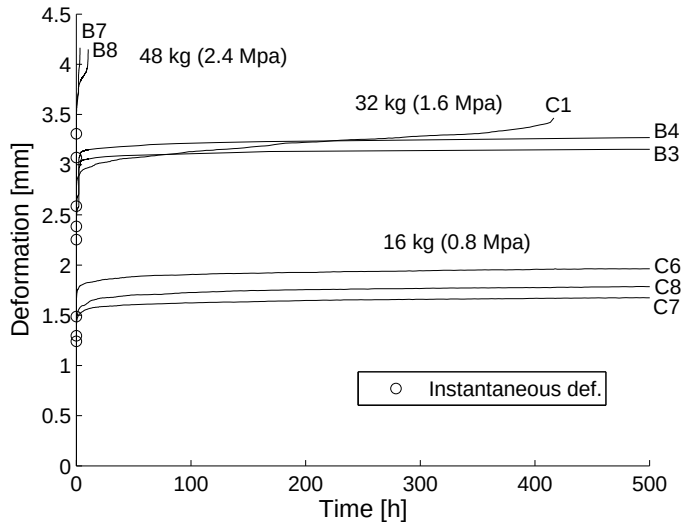

Figure 3.11: *Creep test results of CR rubber, 0-500 h.*

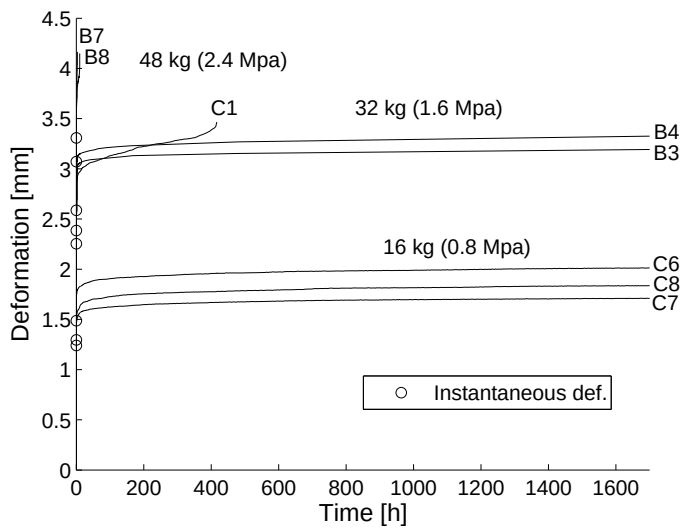

Figure 3.12: *Creep test results of CR rubber, 0-1700 h.*

Table 3.5: *Results of creep test B and C.*

Spec.	Rub.	Load [kg]	τ [MPa]	κ_e [-]	κ_c [-]	t_c [h]	κ_f [-]	t_f [h]	Type of failure r/r-a/w [%]
B1	X	32.23	1.58	1.51	2.30	141	2.70	151	85/15/0
B2	X	32.75	1.61	1.35	2.05	523	2.49	580	100/0/0
B3	CR	32.66	1.60	2.25	-	-	-	>1700	No failure
B4	CR	32.52	1.60	2.39	-	-	-	>1700	No failure
B5	X	48.90	2.40	1.87	-	-	-	2.1	Not in the joint
B6	X	48.37	2.37	1.93	2.34	1.78	2.46	2.1	100/0/0
B7	CR	48.67	2.39	3.31	3.95	2.40	4.15	3.3	90/10/0
B8	CR	48.00	2.35	3.07	3.93	8.80	4.15	10.4	100/0/0
C1	CR	32.23	1.58	2.59	3.30	326	3.47	417	90/10/0
C6	CR	16.49	0.81	1.49	-	-	-	>1700	No failure
C7	CR	16.14	0.79	1.24	-	-	-	>1700	No failure
C8	CR	16.77	0.82	1.30	-	-	-	>1700	No failure

Table 3.6: *Shear strains at stress levels present in the creep tests and failure types of test MWA [9].*

Spec.	Rub.	$\kappa_e(\tau$=0.8) [-]	$\kappa_e(\tau$=1.6) [-]	$\kappa_e(\tau$=2.4) [-]	Type of failure r/r-a/w [%]
CR 1	CR	1.05	2.05	2.80	75/25/0
CR 2	CR	1.85	2.75	3.38	98/2/0
CR 3	CR	1.50	2.45	3.20	80/20/0
CR 4	CR	1.38	2.45	3.20	75/25/0
CR 5	CR	1.35	2.40	3.20	80/20/0
Mean		1.43	2.42	3.16	-
Std		0.29	0.25	0.21	-

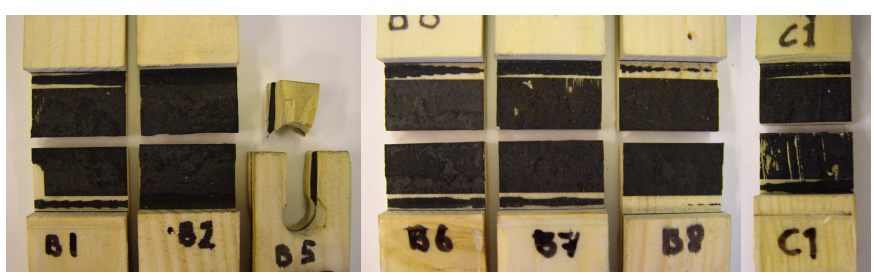

Figure 3.13: *Failure types of the test specimens in the creep test.*

3.4.3 Discussion

The two types of rubber used in the creep test showed different responses during the test. The difference in load between nominally equally loaded specimens is small but the initial shear strains were distinctly larger for CR compared to X, indicating a higher value of the initial shear modulus G_0 for the X-rubber. Furthermore, the rubber deformed in slightly different ways for the X specimens tested compared to the CR specimens which can be seen in Figure 3.14. Since the results of the two rubber types were clearly different, the rubber in the specimens marked X cannot be of the same type as the rubber in specimens with known rubber type. In the development of a material model, only the results of the CR-rubber specimens are therefore used.

The failure of specimen B5 did not occur in the test joint, but was a wood failure at the attachment of the specimen to the loading device. Careful analysis of the test data shows that failure first occurred in specimen B5 and the fall of the almost 50 kg heavy load lead to an immediate failure in specimen B6, where failure most likely was about to occur very soon anyway. The remaining six specimens were also affected by the fall of the first specimen, which can be seen in Figure 3.10 as a sudden increase of elongation at the same time as the fall of specimens B5 and B6. Test C1 shows that the impact of the fall of B5 on specimen B3 and B4 was probably large. Comparison between C1 and B3-B4 leads to the conclusion that most of the creep deformations that were about to occur for specimen B3 and B4 occurred at a short time of extra load. The rate of the creep for B3 and B4 after the impact is probably more valid after long time for the current rubber type. Thus, the results of specimen B3 and B4 are assumed not to be representative for the creep behaviour of the rubber and are therefore not used in the further work of describing the creep behaviour for the material model.

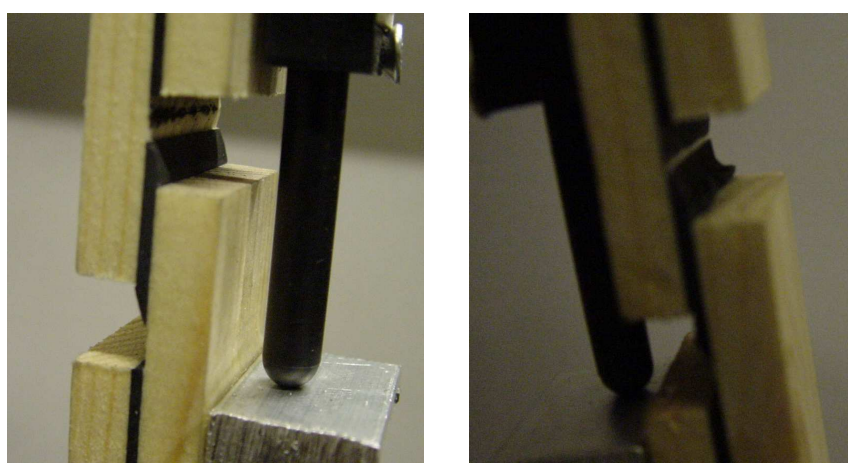

Figure 3.14: *Deformation of CR-rubber (left) and X-rubber (right).*

The short term ramp loading shear strength of the CR-rubber obtained by the stress vs. strain tests presented in Section 3.1 was in average 3.169 MPa, see Table 3.2. This strength corresponds to a weight of 64.6 kg which means that the tests with 48 kg has a load of 74 % of the failure load. In the test results of the stress vs. strain tests, presented in Table 3.2, it can also be seen that the average serviceability limit strain, κ_c, of the test specimens is 2.57 mm corresponding to a stress of 1.77 MPa. This implies that a load of 48 kg (2.4 MPa) is too high when trying to analyse the viscoelastic behaviour of the CR-rubber since the risk of failure being initialised at the shear stresses present is imminent. The results of the creep tests for the specimens with 48 kg load have therefore not been used in the further work of describing the viscoelastic behaviour.

A comparison between the instantaneous strains, κ_e, of the creep tests and the strains in the stress vs. strain test at corresponding stresses shows very good agreement, see Table 3.5 and Table 3.6.

The results of this creep test are evaluated further in section 4.4.

Chapter 4

Development of rubber material models

4.1 Hyperelastic models in serviceability limit state

The development of hyperelastic material models in the serviceability limit state consists of evaluation of the short term ramp loading stress vs. strain performance of test MWA. Material parameters are determined using least square fit of the stress vs. strain relationships for the Neo Hooke and Yeoh strain energy functions.

4.1.1 Method

The least squares fits were done with respect to the absolute error in shear stress for the Neo Hooke and Yeoh stress vs. strain relationships. The expressions for these relationships are given by Equation 2.34 for the Neo Hooke model and Equation 2.38 for the Yeoh model. The least squares fit was performed by setting up an overdetermined system of equations were each equation corresponds to a data point consisting of τ_i^{exp} and κ_i^{exp}. The computations were carried out in MATLAB using the following procedure where n is the number of data points and m the number of coefficients for the hyperelastic material model ($m_{NeoHooke} = 1$ and $m_{Yeoh} = 3$).

$$\mathbf{b} = \mathbf{A}\mathbf{c} \tag{4.1}$$

$$\begin{bmatrix} b_1 \\ b_2 \\ \vdots \\ b_n \end{bmatrix} = \begin{bmatrix} A_{11} & \dots & A_{1m} \\ A_{21} & \dots & A_{2m} \\ \vdots & \ddots & \vdots \\ A_{n1} & \dots & A_{nm} \end{bmatrix} \begin{bmatrix} c_1 \\ \vdots \\ c_m \end{bmatrix} \tag{4.2}$$

The column vector $\mathbf{b}$ contains the recorded shear stresses τ_i^{exp}. In matrix $\mathbf{A}$, A_{i1} indicates $2\kappa_i^{exp}$, A_{i2} indicates $4(\kappa_i^{exp})^3$, A_{i3} indicates $6(\kappa_i^{exp})^5$. The column vector $\mathbf{c}$ contains the sought coeffients. It is impossible to find the inverse of $\mathbf{A}$ since it is not

square ($m \neq n$). Instead, a least squares fit of Equation 4.2 is performed by first multiplying both sides with the transpose of $\mathbf{A}$:

$$\mathbf{A^T b} = \mathbf{A^T A c} \tag{4.3}$$

Both sides of equation 4.3 are then multiplied with the inverse of $(\mathbf{A^T A})$, a $m \times m$ matrix possible to invert.

$$(\mathbf{A^T A})^{-1}\mathbf{A^T b} = (\mathbf{A^T A})^{-1}(\mathbf{A^T A})\mathbf{c} \tag{4.4}$$

Equation 4.5 is the solution in the least squares sense and the hyperelastic coefficients $\mathbf{c}$ are determined with respect to minimize the sums of the squares of the differences between experimental and theoretical stresses at different strain values [2].

$$(\mathbf{A^T A})^{-1}\mathbf{A^T b} = \mathbf{c} \tag{4.5}$$

The fits were made with respect to the three tests (CR 3, CR 4 and CR 5) that were considered to represent the material correctly. Because of the nonlinear behaviour of rubber, the accuracy of the Neo Hooke model (and also the Yeoh model) depends to a large extent on the used stress-strain interval of test data. In order to obtain a linear material model that is accurate for the stress interval assumed to be relevant for practical applications, only this interval should be used when performing the least squares fit to test data. When trying to fit a material model for the serviceability limit state, only data points up to the second inflexion point should be used following the line of reasoning in Subsection 2.3.1. According to Table 3.2, the second inflexion point for CR 3, CR 4 and CR 5 is at a stress level of $\tau \approx 1.77$ MPa. Hence, data points with higher shear stress were omitted when performing the least squares fits. The total number of data points, n, are 632, divided among the three test according to $n_{cr3} = 308$, $n_{cr4} = 163$ and $n_{cr5} = 161$.

Neo Hooke

The over determined system of equations when fitting the Neo Hooke model to test data in the serviceability limit state is obtained from Equation 2.34:

$$\tau = 2C_{10}\kappa \Rightarrow \tag{4.6}$$

$$\begin{bmatrix} \tau_1^{exp} \\ \tau_2^{exp} \\ \tau_3^{exp} \\ \vdots \\ \tau_{632}^{exp} \end{bmatrix} = \begin{bmatrix} 2\kappa_1^{exp} \\ 2\kappa_2^{exp} \\ 2\kappa_3^{exp} \\ \vdots \\ 2\kappa_{632}^{exp} \end{bmatrix} \begin{bmatrix} C_{10} \end{bmatrix} \tag{4.7}$$

Yeoh

The overdetermined system of equations when fitting the Yeoh model to test data in the serviceability limit state is obtained from Equation 2.38:

$$\tau = 2C_{10}\kappa + 4C_{20}\kappa^3 + 6C_{30}\kappa^5 \Rightarrow \tag{4.8}$$

$$\begin{bmatrix} \tau_1^{exp} \\ \tau_2^{exp} \\ \tau_3^{exp} \\ \vdots \\ \tau_{632}^{exp} \end{bmatrix} = \begin{bmatrix} 2\kappa_1^{exp} & 4(\kappa_1^{exp})^3 & 6(\kappa_1^{exp})^5 \\ 2\kappa_2^{exp} & 4(\kappa_2^{exp})^3 & 6(\kappa_2^{exp})^5 \\ 2\kappa_3^{exp} & 4(\kappa_3^{exp})^3 & 6(\kappa_3^{exp})^5 \\ \vdots & \vdots & \vdots \\ 2\kappa_{632}^{exp} & 4(\kappa_n^{exp})^3 & 6(\kappa_n^{exp})^5 \end{bmatrix} \begin{bmatrix} C_{10} \\ C_{20} \\ C_{30} \end{bmatrix} \tag{4.9}$$

4.1.2 Results

The computed coefficients for the two strain energy models are the following:

$$\text{Neo Hooke:} \qquad C_{10} = 0.3050 \qquad \text{MPa} \tag{4.10}$$

$$\text{Yeoh:} \qquad \begin{cases} C_{10} = 0.3146 & \text{MPa} \\ C_{20} = -0.01041 & \text{MPa} \\ C_{30} = 0.001363 & \text{MPa} \end{cases} \tag{4.11}$$

As can be seen in Figure 4.1, the Yeoh model gives an overall better fit to the test data of the used stress-strain interval compared to the Neo Hooke model. The latter, however, shows an acceptable match to the test data for the fitted interval. Since the models are developed using a limited stress-strain interval of the test data, they will not be accurate when trying to determine the load at failure. The developed Neo Hooke and Yeoh material models are shown in Figure 4.2 along with the complete test data for CR 3, CR 4 and CR 5.

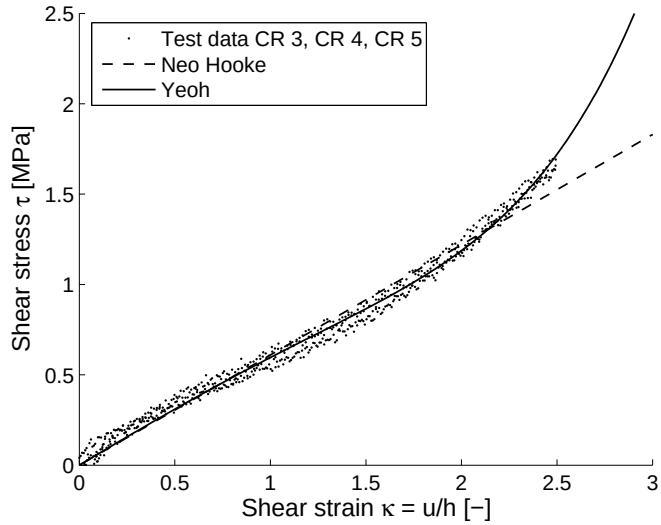

Figure 4.1: *Least squares fit for Yeoh and Neo Hooke models to test data.*

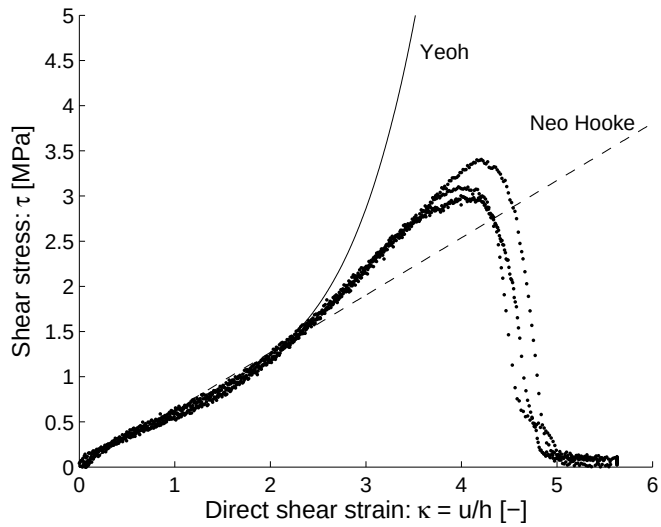

Figure 4.2: *Fitted Neo Hooke and Yeoh material models.*

Stability

The models need also to be stable for strain values outside as well as inside the fitted interval in order to represent a reasonable physical material [2]. A stable

strain energy functions has only one minimum value and this minimum is at the undeformed state where $\lambda_1 = \lambda_2 = \lambda_3 = 1$. When the material is stretched in some way, the strain energy increases. A stable material model must have this property and should therefore only show one minimum value and be bowl-shaped when plotted as a function of λ_1 and λ_2. The hyperelastic material models obtained from the least square fit have these properties as can be seen in Figure 4.3.

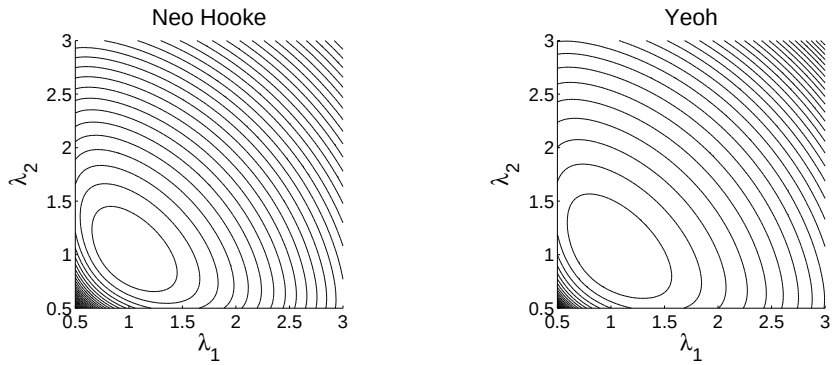

Figure 4.3: *Strain energy density plot for Neo Hooke and Yeoh models.*

4.1.3 Discussion

Previous tests have shown that creep occurs in the CR-rubber already during the first couple of minutes after loading. Since the loading process in the test procedure of test MWA lasted for up to five minutes, the test data does not really describe the instantaneous hyperelastic behaviour. Part of the strains, especially at higher strain levels occurring later in the test, are due to viscoelastic effects which means that the rubber is actually somewhat stiffer at instantaneous loading than shown in the Figure 4.1. This means that the stress vs. strain models and the corresponding material parameters, given in Equation 4.10 and Equation 4.11, are valid for a loading duration in the order of a few minutes rather than truly instantaneous loading.

The aim of the test was to examine the hyperelastic behaviour of rubber. The deformation of the test specimens was recorded as movement of the piston and it was assumed that the recorded deformations took place in the rubber foil, because of the large difference in stiffness between the rubber and the wood. This is not the case however, since FE-analyses show that the wooden parts are exposed to strains that are small but not negligible compared to the strains in the rubber foil. The stress-strain curves shown above are actually not material relationships for rubber but rather a relationship for this particular specimen combined of rubber and wooden parts. The actual hyperelastic relationship for rubber should therefore show a stiffer behaviour. In order to compensate for the strains in the wooden parts and achieve

a true model of the hyperelastic properties for rubber, FE-analyses were carried out in ABAQUS. This is described in Section 4.3.

4.2 Hyperelastic models in ultimate limit state

Since the material models developed in Section 4.1 do not correspond well with test data at higher strain values, other models need to be developed to be able to accurately predict the load at failure for short term loading. Two separate methods of finding a Neo Hooke material model for the ultimate limit state are presented here.

Method 1

For the linear Neo Hooke model, a material model for the ultimate limit state can be obtained using the mean values of τ_f and κ_f from CR 3, CR 4 and CR 5 presented in Table 3.2. Fitting the Neo Hooke model to τ_f and κ_f only, yields a model which will more accurately describe the rubber in the ultimate limit state compared to the model fitted to a limited stress-strain interval. The coefficient C_{10} is determined according to the following equations where G is the shear modulus.

$$G = \frac{\Delta\tau}{\Delta\kappa} = \frac{3.169 - 0}{4.058 - 0} = 0.781\,\text{MPa} \tag{4.12}$$

$$C_{10} = \frac{G}{2} = 0.3905\,\text{MPa} \tag{4.13}$$

Method 2

Another way of determining a material model in the ultimate limit state is to consider the fracture energy G_f and the maximum shear stress τ_f. Imposing a constraint saying that the model has the same fracture energy as the mean fracture energy of tests CR 3, CR 4 and CR 5 from Table 3.2 and also that the shear stress τ_f is the same for the model and the tests will yield a fictitious failure strain κ_f. Equation 2.50 and Equation 2.51 can be used to determine the fictitious failure strain κ_f.

$$G_f = 0.0076\,\text{MN/m} \tag{4.14}$$

$$G_f = t\int_0^{\kappa_f} \tau\, d\kappa = t\,\frac{1}{2}\tau_f\kappa_f \tag{4.15}$$

$$\Rightarrow \kappa_f = \frac{2 \cdot G_f}{t \cdot \tau_f} = 4.796 \tag{4.16}$$

From these two variables (τ_f and κ_f), the Neo Hooke coefficient C_{10} can easily be determined in the same manner as used in method 1 above.

$$G = \frac{\Delta\tau}{\Delta\kappa} = \frac{3.169 - 0}{4.796 - 0} = 0.661\,\text{MPa} \tag{4.17}$$

$$C_{10} = \frac{G}{2} = 0.3305\,\text{MPa} \tag{4.18}$$

The models according to method 1 and method 2 are shown in Figure 4.4.

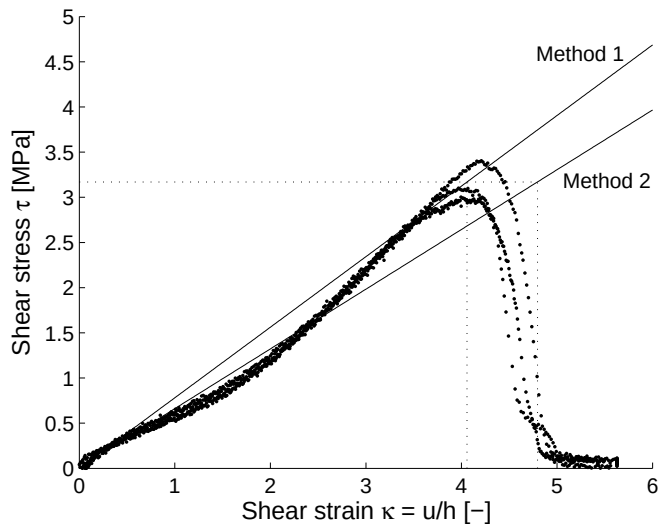

Figure 4.4: *Fitted Neo Hooke models according to method 1 and method 2.*

4.3 Calibration of hyperelastic models

In order to achieve more accurate models for the hyperelastic behaviour of the CR rubber, an FE-analysis of stress vs. strain performance of test MWA was carried out. The material parameters obtained from the least squares fits in Section 4.1 were calibrated by comparison between the results of FE-analyses and the experimental test.

4.3.1 Method

The geometry and setup of test MWA is briefly described in Section 3.1. To be able to model the applied load and boundary conditions with sufficient accuracy, the steel plates used to fixate the test piece were also modelled although rather simplified. The symmetry of the test piece was used to decrease the number of elements and the time duration for the calculations. Analyses were first made with 270 elements

in the rubber foil but the model shown in Figure 4.5 with only nine elements was considered to be accurate enough, since the difference in shear strain in the rubber foil was less than 1 %. The elements used for the rubber parts were hybrid (mixed formulation), linear displacement, 8-node brick elements with 3 degrees of freedom per node (denoted C3D8H in ABAQUS) and standard, linear displacement, 8-node brick elements with 3 degrees of freedom per node for the wooden- and steel parts (denoted C3D8 in ABAQUS).

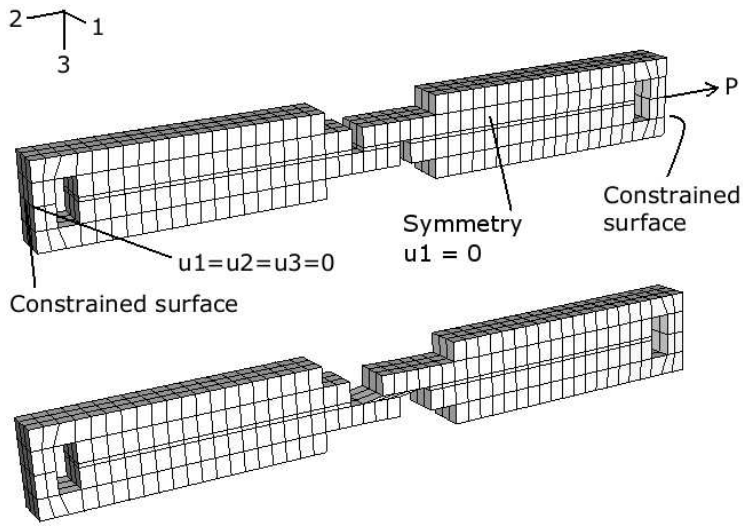

Figure 4.5: *Finite element model of test piece used in test MWA, undeformed and deformed.*

The actual test was run with a constant rate of increase in displacement and recording of the applied force necessary for these displacements. The FE-analysis was instead carried out with a constant rate of increase in applied force. However, this difference should not have an impact on the results.

The coefficients for the Neo Hooke and the Yeoh material model according to Equation 4.10 and Equation 4.11 were used as an initial description of the hyperelastic properties. Unadjusted, the coefficients will yield deformations in the rubber foil that are equal to the total deformations (rubber foil and wood) in the test specimen. The straining in the wood will therefore be added twice and the total deformation will be too large. Thus, the coefficients needs to be increased to a point where the total deformations of the FE-model corresponds to the recorded deformations of test MWA. Having done this, the hyperelastic coefficients truly describe the hyperelastic behaviour of the rubber only and not the behaviour of the test specimens combined of rubber and wooden parts. The following procedure was used to compensate for the strains in the wooden parts of the specimen.

1. An FE-analysis was carried out and the deformation was recorded as global

elongation and as elongation of the rubber foil. For the global measuring, the elongation was defined as $u_2^{G1} - u_2^{G2}$ and for the rubber measuring as $u_2^{R1} - u_2^{R2}$. Figure 4.6 shows the position of the points $G1$, $G2$, $R1$ and $R2$.

2. The stiffness of the rubber was then increased in order to get the globally measured elongation to agree with the elongation of the rubber foil computed with the unadjusted constants. For the 3-parameter Yeoh model, this was done by multiplying all coefficients with the same factor and for the Neo Hooke model by simply increasing the one coefficient.

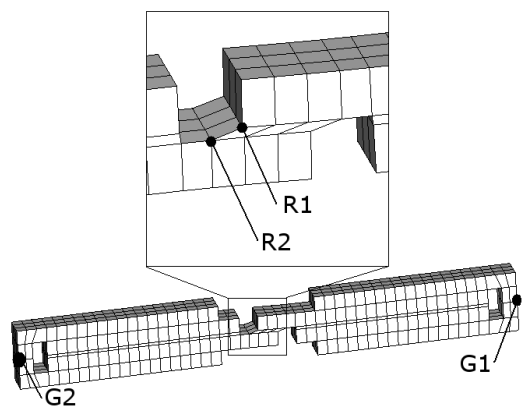

Figure 4.6: *Global measurement and rubber measurement.*

4.3.2 Materials

Wood

The wooden parts of the specimens consist of Swedish fir and were modelled as an orthotropic material with linear elastic properties according to Table 4.1. Young's modulus E, the shear modulus G and Poison's ratio ν was specified in the three material directions; longitudinal (L), radial (R) and tangential (T) to grain.

Table 4.1: *Used material parameters for wooden parts [5].*

Young's Modulus E MPa	Shear Modulus G MPa	Poisson's ratio ν -
$E_L = 14000$	$G_{RL} = 600$	$\nu_{RL} = 0.02$
$E_R = 800$	$G_{TL} = 700$	$\nu_{TL} = 0.02$
$E_T = 500$	$G_{TR} = 60$	$\nu_{TR} = 0.3$

For the model in Figure 4.5, material directions were given as longitudinal in the length (2), tangential in the width (1), and radial in the height (3) of the specimen.

Steel

The steel was modelled as an isotropic material with Young's modulus $E = 210$ GPa and Poisson's ratio $\nu = 0.3$.

Adhesive

Full interaction was assumed between the rubber foil and wooden parts. The analysis was thus simplified by ignoring the presumably very small deformations in the adhesive bond.

Rubber

The coefficients for the Neo Hooke and the Yeoh material model according to Equation 4.10 and Equation 4.11 were used as an initial definition of the hyperelastic behaviour. These coefficients were then increased as described above.

4.3.3 Results

The two models gave an acceptable match to test data when their respective coefficients were increased 4 % yielding the hyperelastic coefficients according to Equation 4.19 and Equation 4.20. The calibrated Neo Hooke and Yeoh material models are presented in Figure 4.7 and Figure 4.8.

$$\text{Neo Hooke:} \qquad C_{10} = 0.3172 \quad \text{MPa} \tag{4.19}$$

$$\text{Yeoh:} \qquad \begin{cases} C_{10} = 0.3272 & \text{MPa} \\ C_{20} = -0.01083 & \text{MPa} \\ C_{30} = 0.001418 & \text{MPa} \end{cases} \tag{4.20}$$

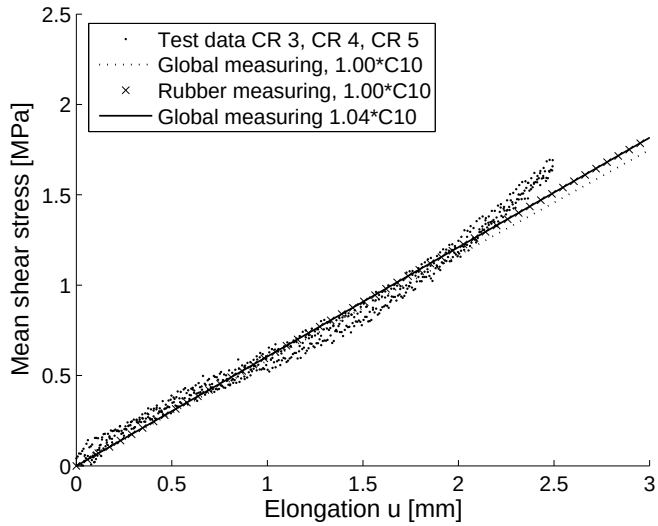

Figure 4.7: *Neo Hooke calibrated model.*

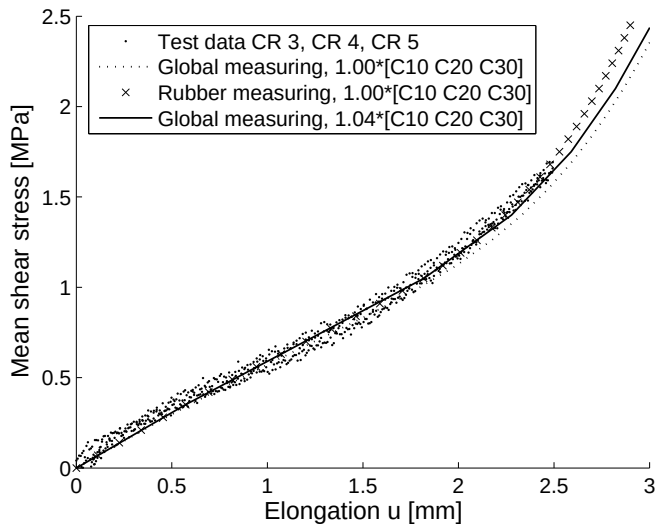

Figure 4.8: *Yeoh calibrated model.*

4.3.4 Discussion

As can be seen in Figure 4.7 and Figure 4.8, the results for the calculations with global measuring and adjusted coefficients correspond well to the results of the calculations with rubber measuring and unadjusted coefficients. This indicates that the calibrated material models describe the behaviour of rubber rather than the behaviour of the complete specimen.

One condition for this procedure to work is of course that the material model used for the wooden parts is reasonably accurate. Fulfilment of this criterion has not been checked by tests. The procedure is, however, not very sensitive to the stiffness of the wood and the presently used material data is believed to be sufficiently accurate.

4.4 Viscoelastic models

The development of viscoelastic models consists of evaluating the results from the creep tests and finding a viscoelastic material model that can be used in Neo Hooke FE-analyses. In order to use the model in conjunction with the Yeoh model, the model has to be adjusted according to Subsection 2.2.4. It has been shown in Subsection 2.1.3 that a generalised Maxwell model can be useful when trying to find an appropriate description of the viscoelastic behaviour. Using this approach will not only yield a set of prony coefficients, but also an indication of the initial stiffness G_0 of the rubber. Tests C1, C6, C7 and C8 were the only ones out of the 12 performed creep tests that were considered successful, see Subsection 3.4.3. Hence, these four are the ones evaluated in this chapter.

4.4.1 Method

Computations were carried out using MATLAB and functions written by the authors for the different steps in the procedure. The material is described by a rheological generalised Maxwell model of springs and dashpots according to Figure 2.5 and the corresponding equations used are presented below.

$$G_R(t) = G_0 - \sum_{i=1}^{N} G_i(1 - e^{-t/t_{ri}}) \tag{4.21}$$

$$G_R(t) = \frac{\tau}{\kappa(t)} \tag{4.22}$$

$$g_R(t) = \frac{G_R(t)}{G_0} \tag{4.23}$$

$$g_i = \frac{G_i}{G_0} \tag{4.24}$$

$$G_\infty = G_0(1 - \sum_{i=1}^{N} g_i) \tag{4.25}$$

$$C_{10,NeoHooke} = \frac{G_0}{2} \tag{4.26}$$

The procedure used for calculating the prony coefficients is the following:

1. The number N of Maxwell elements in the rheological model and their individual relaxation times were chosen. According to [4], the number of Maxwell elements should be less or equal to $\log t_{max}/t_{min}$. Concerning the choice of relaxation times, several different sets need to be tested before deciding on which one gives the best fit. The chosen number N of Maxwell elements and their individual relaxation times t_{ri} can be seen in Table 4.2.

2. The overdetermined system of equations, according to Equation 4.21 and Equation 4.22, for the n data points was set up:

$$\frac{\tau}{\kappa(t)} = G_0 - \sum_{i=1}^{N} G_i(1 - e^{-t/t_{ri}}) \tag{4.27}$$

$$\begin{bmatrix} \tau_0/\kappa(t_1) \\ \tau_0/\kappa(t_2) \\ \tau_0/\kappa(t_3) \\ \vdots \\ \tau_0/\kappa(t_n) \end{bmatrix} = \begin{bmatrix} 1 & -(1-e^{-t_1/t_{r1}}) & \dots & -(1-e^{-t_1/t_{rN}}) \\ 1 & -(1-e^{-t_2/t_{r1}}) & \dots & -(1-e^{-t_2/t_{rN}}) \\ 1 & -(1-e^{-t_3/t_{r1}}) & \dots & -(1-e^{-t_3/t_{rN}}) \\ \vdots & \vdots & \ddots & \vdots \\ 1 & -(1-e^{-t_n/t_{r1}}) & \dots & -(1-e^{-t_n/t_{rN}}) \end{bmatrix} \begin{bmatrix} G_0 \\ G_1 \\ \vdots \\ G_N \end{bmatrix} \tag{4.28}$$

$$\mathbf{b} = \mathbf{A}\,\mathbf{c} \tag{4.29}$$

3. The overdetermined system of equation was solved using least squares in the same way as described in Subsection 4.1.1:

$$\mathbf{A^T b} = \mathbf{A^T A c} \tag{4.30}$$

$$(\mathbf{A^T A})^{-1}\mathbf{A^T b} = (\mathbf{A^T A})^{-1}(\mathbf{A^T A})\mathbf{c} \tag{4.31}$$

$$(\mathbf{A^T A})^{-1}\mathbf{A^T b} = \mathbf{c} \tag{4.32}$$

4. The prony coefficients g_i were then determined according to equation 4.24.

To make sure that the chosen number of Maxwell elements and the chosen relaxation times gave a good fit to the experimental data, the shear strain $\kappa(t)$ was plotted over the time interval t_{min} to t_{max} using Equation 4.21 and Equation 4.22 for the different shear stress levels. The result was then compared to the experimental data. The dimensionless relaxation modulus $g_R(t)$ was also plotted. The choice of relaxation times has a great impact on the results of the computations. The final choice was made with respect to getting an overall well-fitted curve with extra attention given to the later part in the tests. The shear modulus at t_∞ is

given by Equation 4.25 and the initial Neo Hooke coefficient C_{10} is given by Equation 4.26. The hyperelastic Neo Hooke coefficients achieved from the creep tests include straining in the wooden parts. In order to make them describe the deformations in the rubber foil only, they were multiplied with a factor 1.04 which was iteratively acquired in Section 4.3.

Each test was first individually analysed. Since there are differences between the tests, each set of prony coefficients obtained describes the decrease in stiffness over time well for the specific test but not so well for another test. In order to achieve a single set of prony coefficients that will result in an acceptable behaviour for all stress levels, the tests were also analysed together. Since there was only one successful test at the load level of 32 kg, an analysis was made with the test data from C1 used three times and the test data from C6, C7 and C8 used once each.

Common for all calculations is that values from the first minute of each test are ignored. The reason for this is to compensate for the small creep strains included in the hyperelastic parameters obtained from test MWA. This implies that the material model should give an instantaneous deformation that is slightly too large but a precise value of deformation for long-term loading.

4.4.2 Results

The results of the least squares fit to test data from creep test can be seen in Figure 4.9 and Figure 4.10 for different time scales. The computed relaxation moduli $g_R(t)$ can be seen in Figure 4.11. Table 4.2 presents the chosen relaxation times t_{ri}, the computed prony coefficients g_i and instantaneous Neo Hooke coefficients C_{10}.

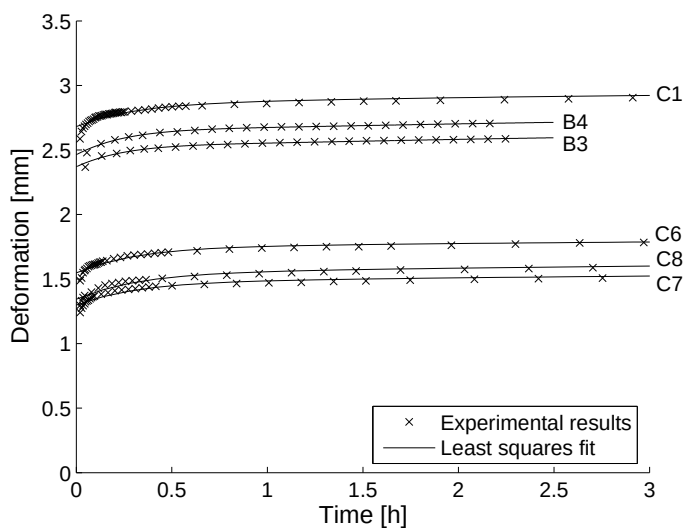

Figure 4.9: *Least squares fit to creep test data, 0-3 h.*

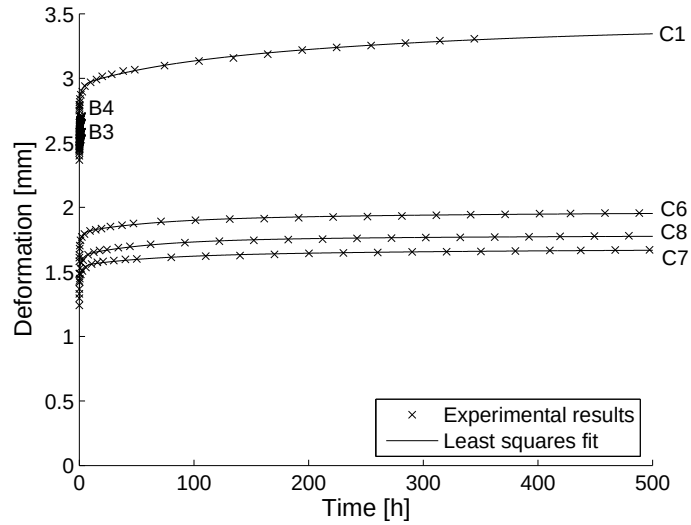

Figure 4.10: *Least squares fit to creep test data, 0-500 h.*

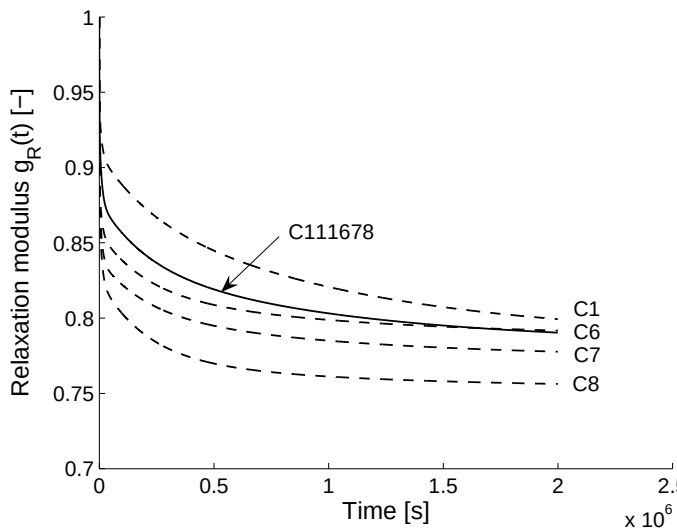

Figure 4.11: *Relaxation modulus* $g_R(t)$.

Table 4.2: *Computed prony coefficients and corresponding relaxation times.*

	g_1 [-] $t_{r1} = 10^3$ [s]	g_2 [-] $t_{r2} = 10^4$ [s]	g_3 [-] $t_{r3} = 2 \cdot 10^5$ [s]	g_4 [-] $t_{r4} = 10^6$ [s]	C_{10} [MPa]	$1.04 \cdot C_{10}$ [MPa]
B3	-	-	-	-	0.3380	0.3515
B4	-	-	-	-	0.3238	0.3368
C1	0.05867	0.03186	0.03139	0.09109	0.2947	0.3065
C6	0.10869	0.03462	0.03966	0.02924	0.2613	0.2718
C7	0.11387	0.04747	0.03460	0.03049	0.3048	0.3170
C8	0.12369	0.05094	0.05202	0.01975	0.3060	0.3182
B34C1678	-	-	-	-	0.3048	0.3170
C111678	0.07255	0.04993	0.04050	0.05397	-	-

4.4.3 Discussion

The creep deformations in the tests consist of creep of both the rubber and the wood. Since the creep in the wooden parts of the specimen are approximately less than one percent of the total creep, this creep is considered as negligible. The prony coefficients are therefore treated as describing the creep in the rubber only in the later calibration of the viscoelastic models.

Table 4.2 shows that the Neo Hooke coefficient C_{10} calculated as a mean value of the Neo Hooke coefficients of creep test B3, B4, C1, C6, C7 and C8 is very similar to the unadjusted Neo Hooke coefficient obtained from test MWA according to Equation 4.10. In the calibration of the viscoelastic models, only the modified Neo Hooke coefficient from test MWA according to Equation 4.19 will therefore be tested.

4.5 Calibration of viscoelastic models

In order to calibrate the material models for the viscoelastic behaviour, FE-analyses of the creep test were carried out.

4.5.1 Method

The test specimens and the setup used for the creep test are presented in Section 3.4. Since there was no reason to model any part of the test setup except for the test specimen itself, the model was physically smaller than the model in the analysis in Section 4.3. Hence, the complete geometry could be modelled with reasonable calculation time.

The applied load and boundary conditions were a point load acting on the center of one end area of the model and a fixed support at the center of the unloaded end area. A constraint was applied at each end, forcing the displacement degrees of freedom (u_1, u_2 and u_3) of the constrained area to follow the displacement and rotation of the center point of the end area.

In order to check how fine element mesh was needed, calculations with 15 and 450 elements in the rubber foil were carried out. Since the difference in straining of the rubber foil was less than 1 %, the model with 15 elements was used for the rest of the calculations. The model can be seen in Figure 4.12, undeformed and deformed.

The deformations were recorded as relative displacement between two points corresponding to the points where deformation was measured in the experimental tests. Type of elements and material definitions for wood were the same as presented in the FE-analysis in Section 4.3. Viscoelastic properties are not used for the wooden parts of the specimen since they are assumed to be exposed to relatively small creep strains.

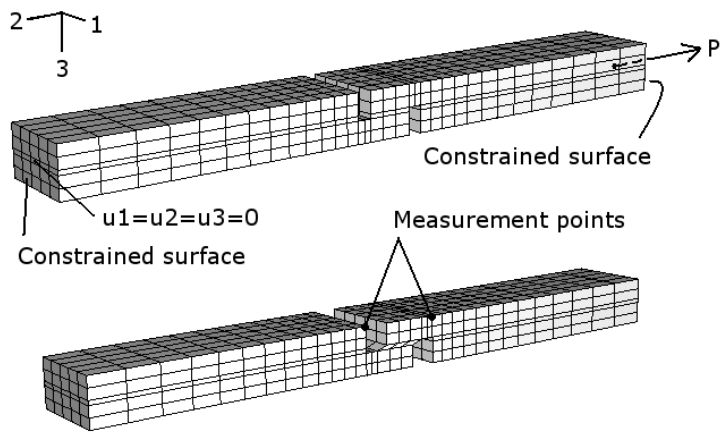

Figure 4.12: *FE-model of specimen for creep test, undeformed and deformed.*

Several different material models were tested in the FE-analyses. The acquired hyper- and viscoelastic parameters were used in different combinations in order to achieve the best possible material model. In order to evaluate the FE-model, computations were carried out with prony coefficients and the modified Neo Hooke constant obtained from each of the tests C1, C6, C7 and C8, according to Table 4.2. If the results of the FE-calculations coincided or were close to the experimental results, the FE-model could be considered as reliable.

Furthermore, the modified Neo Hooke and the Yeoh hyperelastic constants, obtained in Chapter 4.3, were tested in conjunction with the viscoelastic prony coefficients from the least squares fit of all the creep tests C1, C6, C7 and C8 (denoted C111678).

A condition for using the Yeoh model with viscous effects in ABAQUS is that the prony coefficients are multiplied with the factor k. The reason for this condition is explained in Section 2.2.4. Equation 2.48 yields a relationship between k and shear stress τ for the actual rubber as presented in Figure 4.13.

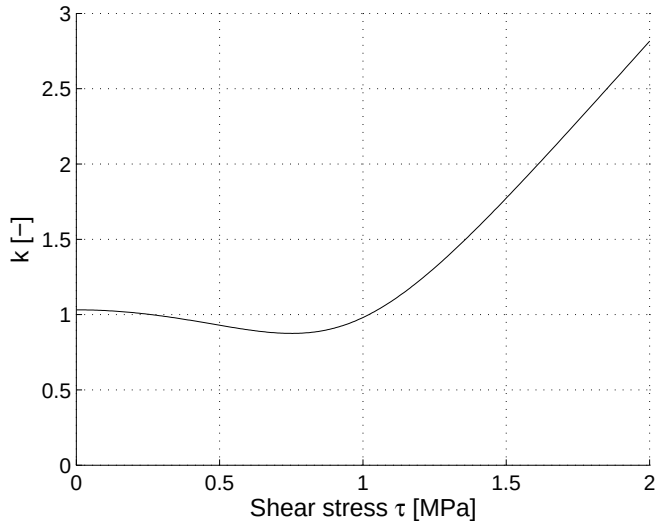

Figure 4.13: *Relationship between k and shear stress τ for used Neo Hooke and Yeoh material models.*

The factor k for the actual stress levels are obtained from Figure 4.13 and are the following:

$$16\,\text{kg load } (0.8\text{ MPa}) \Rightarrow k = 0.878$$
$$32\,\text{kg load } (1.6\text{ MPa}) \Rightarrow k = 1.935$$

For the simulation of the creep test with a load of 48 kg corresponding to an average shear stress of $\tau_c = 2.35$ MPa, only hyperelastic response was analysed since the risk of failure being initialised immediately after loading was considered to be high due to the average shear stress being well above the serviceability limit of $\tau_c = 1.77$ MPa.

4.5.2 Materials

Wood and adhesive

For the wood and adhesive, the material models described in Subsection 4.3.2 were used.

Rubber

The six different rubber material models tested are presented in Table 4.3. The viscoelastic parameters g_i and t_{ri} are presented in table 4.2 and the hyperelastic Neo Hooke and Yeoh coefficients are according to Equation 4.19 and Equation 4.20.

Table 4.3: *Material models used for the FE-analyses of the creep tests. The values of the parameters can be found in Table 4.2*

Nr	Hyperelasticity	Viscoelasticity
1	Neo Hooke C_{10} from C1	g_i and t_{ri} from test C1
2	Neo Hooke C_{10} from C6	g_i and t_{ri} from test C6
3	Neo Hooke C_{10} from C7	g_i and t_{ri} from test C7
4	Neo Hooke C_{10} from C8	g_i and t_{ri} from test C8
5	Neo Hooke C_{10} from MWA	g_i and t_{ri} from test C111678
6	Yeoh C_{10}, C_{20}, C_{30} from MWA	$g_i \cdot k$ and t_{ri} from test C111678

4.5.3 Results

In the figures of the results, the curve number corresponds to the material model number in Table 4.3. For the models tested with different loads, the curves are numbered with a) for the 16 kg load, b) for the 32 kg load and c) for the 48 kg load. Figure 4.14 shows the results of the FE-calculations for material model 1-4, Figure 4.15 and Figure 4.16 show the results of the calculations for material models 5-6, of which the first is provided to clarify the results of the first three hours. The results for the simulation with a load of 48 kg are only provided in Figure 4.15 where the results for the experimental creep test with 48 kg load are presented.

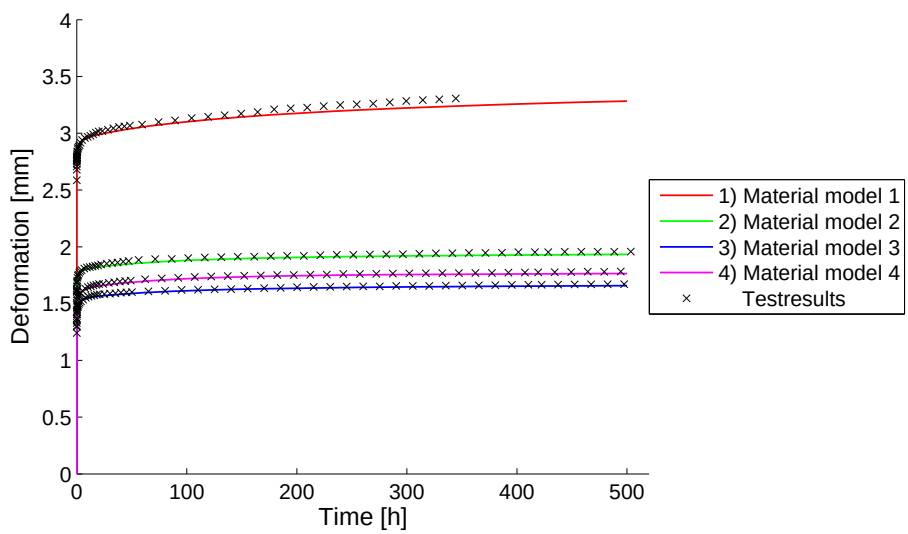

Figure 4.14: *Results of FE-calculations for material model 1-4.*

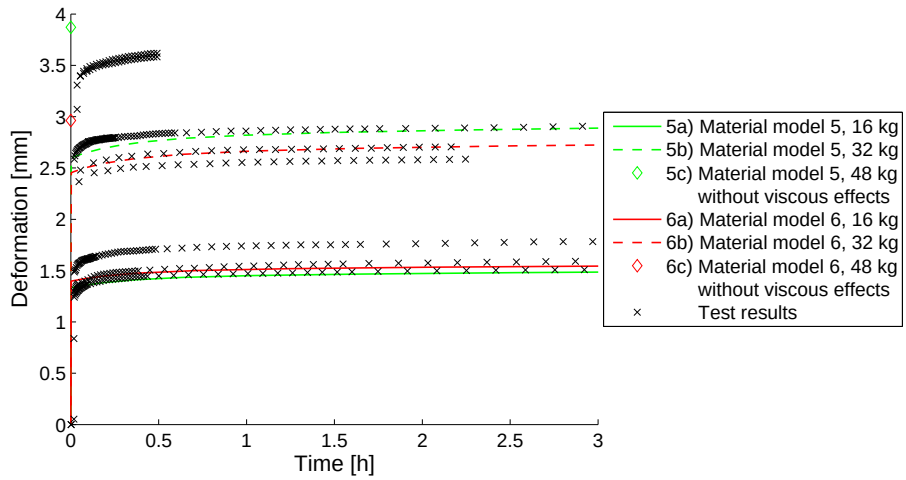

Figure 4.15: *Results of FE-calculations for material model 5-6 for 3 h.*

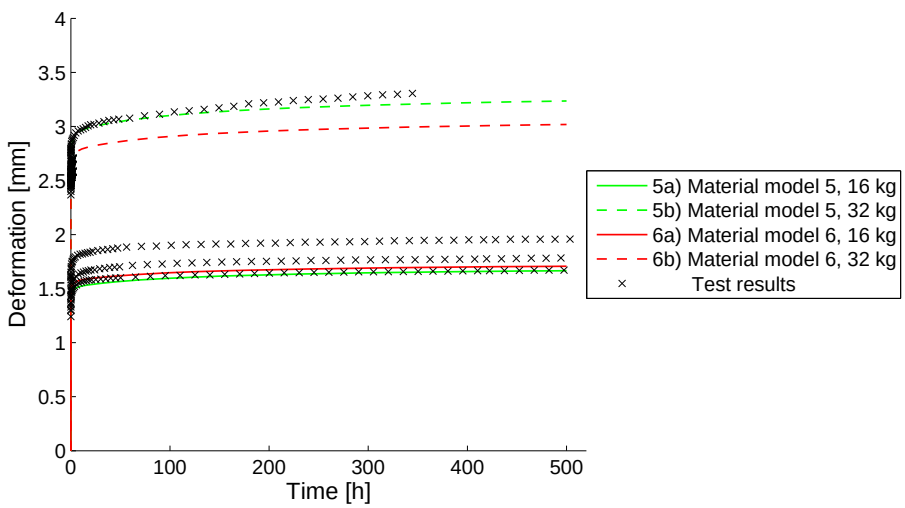

Figure 4.16: *Results of FE-calculations for material model 5-6 for 500 h.*

4.5.4 Discussion

As can be seen in Figure 4.14, the results from the FE-calculations are close to the test results. Curve 2, 3 and 4 almost coincide with the experimental test results and curve 1 is fairly close to the test results on which the material model for this calculation is based. However, all four curves show a creep rate that is slightly too low which is especially visible for curve 1. This could be explained by the small amount of creep that occurred in the wood during the creep tests.

The hyperelastic constants are modified in order to be valid for the rubber only. Thus, the combination of the modified hyperelastic constants and the viscoelastic prony coefficients will yield a creep rate that is slightly lower than for the actual creep tests since the stiffness of the wood is not decreased over time. This implies that the results for material model 1-4 are satisfying since the goal of the development of a viscoelastic material model is to achieve a material model that describes the rubber only. Better correlation between FE-analyses and experimental tests would probably have been achieved if the wooden parts also had been modelled with proper viscoelastic properties.

Figure 4.15 and Figure 4.16 show that each of the material models 5 and 6 give a good description of the hyperelastic behaviour. The instantaneous deformation of the two models are within the range of the instantaneous deformations for the creep tests with 16 kg and 32 kg load. However, comparison between the two models in Figure 4.15 shows that the instantaneous deformation for the Yeoh model is closer to the middle of the instantaneous deformations for the creep tests than it is for the Neo Hooke model. Moreover, the instantaneous deformation for the Yeoh model with 48 kg load is closer to the the test results compared to the Neo Hooke model with the same load.

Figure 4.16 also shows that the creep rates of material model 5 and 6 are the same or very close to one another. This is made possible through the modification of the prony coefficients by the factor k used in conjunction with the Yeoh model for the hyperelasticity.

Furthermore, Figure 4.16 also shows that the creep rate for the FE-calculations differs from the creep rate of the experimental tests. The creep rate of the FE-analyses is lower for the 32 kg tests and slightly higher for the 16 kg tests compared to the experimental results. The reason for this difference is that the prony coefficients are obtained by a least squares fit of test C6, C7, C8 and $3 \cdot$ C1 all together.

4.6 Verification of hyperelastic models

In order to verify the validity of the hyperelastic material models developed previous in this chapter, an FE-analysis of the full-scale beam of test MWF presented in Chapter 3 was carried out.

4.6.1 Method

A model of the full-scale beam was created in ABAQUS. In order to decrease the number of elements and the time of calculation, symmetry was used.

As can be seen in Figure 3.4 and Figure 3.5, the applied load is a pointload, P, acting on a steel profile dividing the load into two point loads acting on the beam. The vertical deformations were recorded by a gauge placed on the steel profile where the load was applied.

The FE-model was simplified by ignoring the steel profile and letting two point loads act directly on the beam. Since the steel profile was not modelled, the deformations needed to be analysed at some other point in the model. This was chosen to be done by using an average value of the vertical deformations at the two points where the loads were applied. In order to decrease the risk for local compression at the points where the loads are applied, two brick-shaped steel plates were modelled on the beam and the point loads were then acting on these. Each of the two loads were ramped linearly from 0 kN to 5 kN, which corresponds to one load ramped from 0 N to 20 kN acting on the complete geometry. The FE-model with boundary conditions and applied loads can be seen in Figure 4.17.

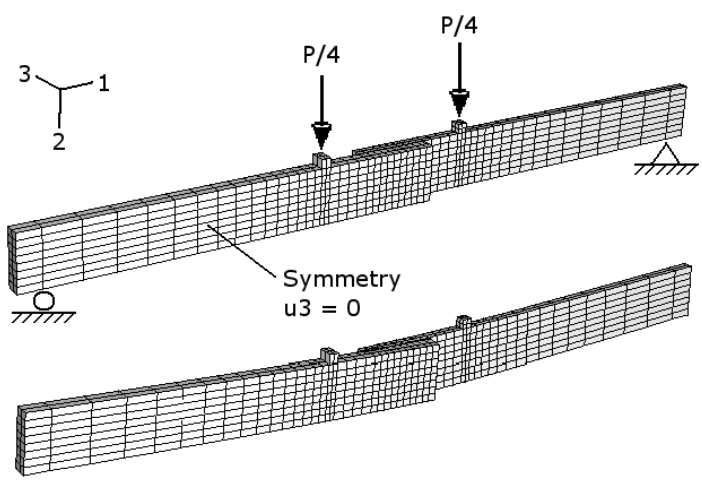

Figure 4.17: *FE-model of test specimen used in test MWF, undeformed and deformed.*

The type of elements used in the calculations are the same as used in the previous FE-analyses presented in this chapter, although with reduced integration. Material data for wood and steel parts are also identical to the previously used data. Longitudinal direction of grain was modelled in the length direction (1), tangential in the height direction (2) and radial in the thickness direction (3) of the beam. Switching directions between tangential and radial made only a very small difference in deformation. Because of the size of the tested beams, the grain orientation in the FE-models are simplified in comparison to the actual beams. A convergence test showed that 80 elements in the rubber layer was a fine enough mesh. The difference in vertical deformations when using 6000 elements compared to 80 elements was less than 1 %.

The shear strain κ and also the shear stress τ were analysed in the mostly stressed areas of the rubber foil, which are the four corner elements shown in Figure 4.18. The shear strain κ in plane with the rubber foil was computed from the relative displacements u_1 and u_2 between the two nodes of the edge corner of the analysed elements. The shear stresses were computed according to:

$$\tau = \sqrt{\tau_{13}^2 + \tau_{23}^2} \tag{4.33}$$

where τ_{13} and τ_{23} are the shear stresses in plane with the rubber foil at the integration points of the analysed elements. Note that the shear strains and shear stresses are not evaluated at the same point.

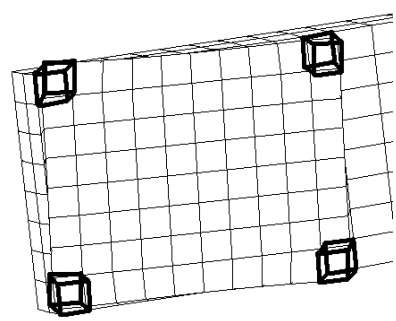

Figure 4.18: *Analysed elements in the rubber foil.*

Verification in ultimate limit state

For verification in the ultimate limit state, the two Neo Hooke models according to Equation 4.34 and Equation 4.35 developed in Section 4.2 were used in the FE-analyses. These models will not necessarily yield an accurate load-displacement graph but should result in an accurate load at failure. It is assumed that complete failure occurs when all four corners of the rubber foil are exposed to shear strains larger than or equal to κ_f.

$$\text{Neo Hooke method 1:} \qquad C_{10} = 0.3905 \qquad \text{MPa} \tag{4.34}$$

$$\text{Neo Hooke method 2:} \qquad C_{10} = 0.3305 \qquad \text{MPa} \tag{4.35}$$

Verification in serviceability limit state

The material models developed in Section 4.3 for the serviceability limit state are designed to be accurate at lower stress-strain values but not necessarily accurate when determining the load at failure. The used hyperelastic models should result in an accurate behaviour of the load-displacement relationship up to the strain limit κ_c for the serviceability state. The calibrated Neo Hooke and Yeoh models according to Equation 4.36 and Equation 4.37 were used in these analyses.

$$\text{Neo Hooke:} \qquad C_{10} = 0.3172 \qquad \text{MPa} \tag{4.36}$$

$$\text{Yeoh:} \qquad \begin{cases} C_{10} = 0.3272 & \text{MPa} \\ C_{20} = -0.01083 & \text{MPa} \\ C_{30} = 0.001418 & \text{MPa} \end{cases} \tag{4.37}$$

4.6.2 Results

Figure 4.19 and Figure 4.20 show the load-displacement graphs for the FE-analyses in the ultimate and the serviceability limit state along with the test results of test MWF. The ultimate loads and deflections at ultimate loads for the hyperelastic material models according to method 1 and method 2 are presented in Table 4.4 which also contains results from the experimental tests.

Table 4.4: *Ultimate loads P_{max} and deflection at ultimate load δ_{Pmax}.*

	κ_f	P_{max} [kN]	δ_{Pmax} [mm]
Test FCR 1		18.53	36.75
(Test FCR 2		13.63	26.17)
Test FCR 3		15.75	32.62
Neo Hooke method 1	4.058	13.27	25.05
Neo Hooke method 2	4.796	13.56	(27.9)

Figure 4.21 and Figure 4.22 show the shear stresses τ_{13} and τ_{23} in the rubber foil for the Yeoh model at a load of 14 kN. The shear strain κ and the shear stress τ at the four corners of the rubber foil are presented as a function of the ramped load in Figures 4.23, 4.24, 4.25 and 4.26 for the four different hyperelastic material models. The shear strain serviceability limit $\kappa_c = 2.57$ is reached at a load of ≈ 7 kN for both models.

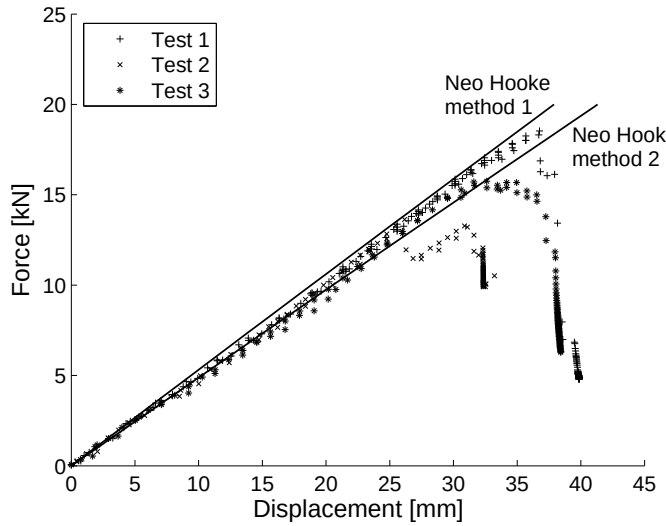

Figure 4.19: *Comparison between test results and FE-analysis, ultimate limit state.*

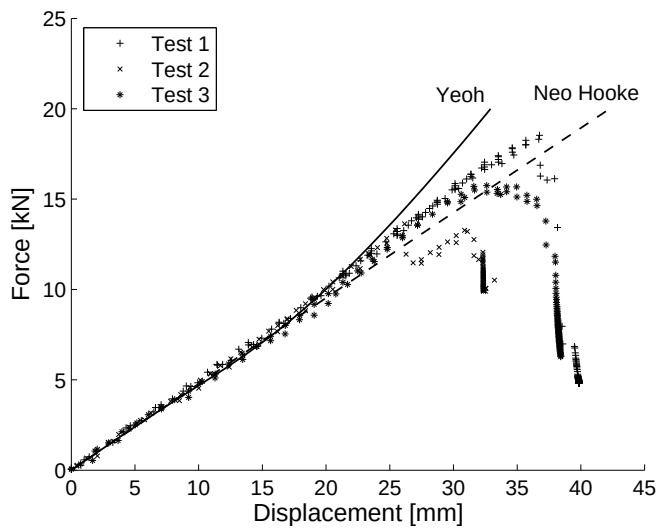

Figure 4.20: *Comparison between test results and FE-analysis, serviceability limit state.*

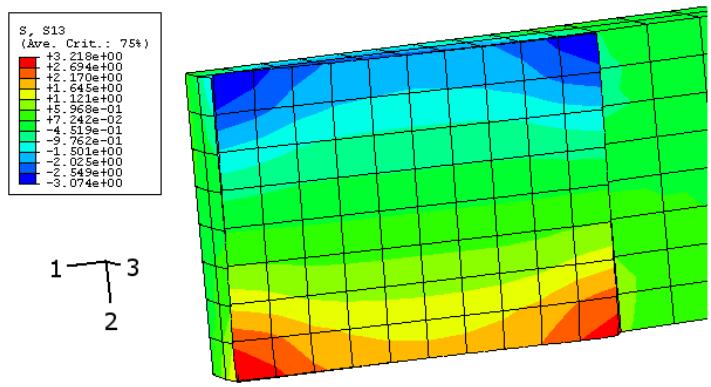

Figure 4.21: *Shear stresses τ_{13} in rubber foil for Yeoh material model at 14 kN.*

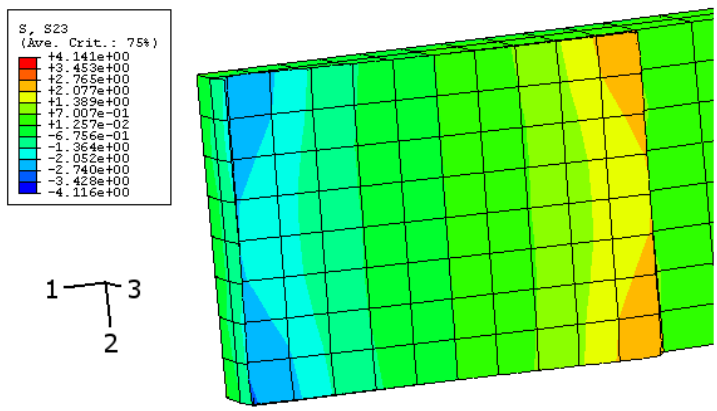

Figure 4.22: *Shear stresses τ_{23} in rubber foil for Yeoh material model at 14 kN.*

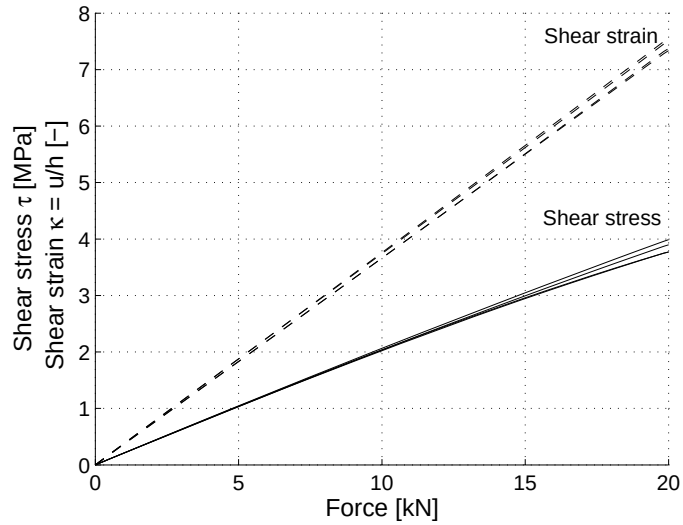

Figure 4.23: *Shear stresses* $\tau = \sqrt{\tau_{13}^2 + \tau_{23}^2}$ *at the integration points of the corner elements and shear strains* κ *in the four corners of the rubber foil for Neo Hooke material model in serviceability limit state.*

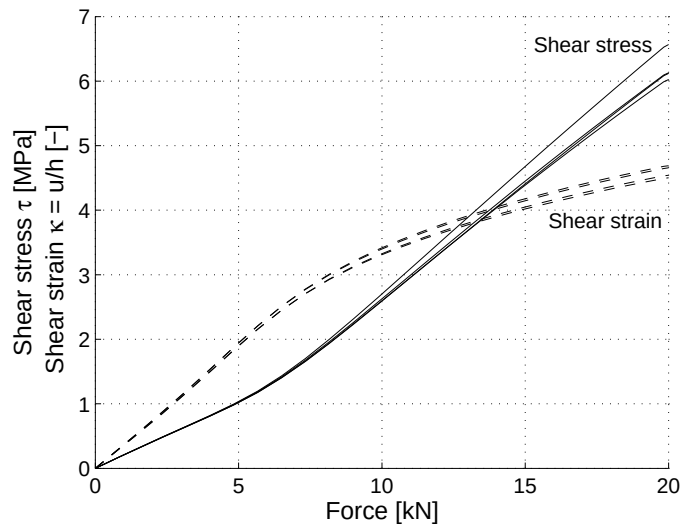

Figure 4.24: *Shear stresses* $\tau = \sqrt{\tau_{13}^2 + \tau_{23}^2}$ *at the integration points of the corner elements and shear strains* κ *in the four corners of the rubber foil for Yeoh material model in serviceability limit state.*

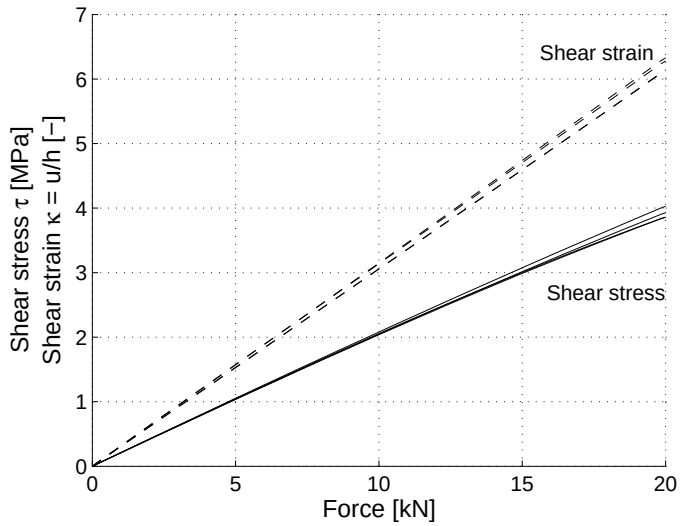

Figure 4.25: *Shear stresses* $\tau = \sqrt{\tau_{13}^2 + \tau_{23}^2}$ *at the integration points of the corner elements and shear strains* κ *in the four corners of the rubber foil for Neo Hooke ultimate limit material model (method 1).*

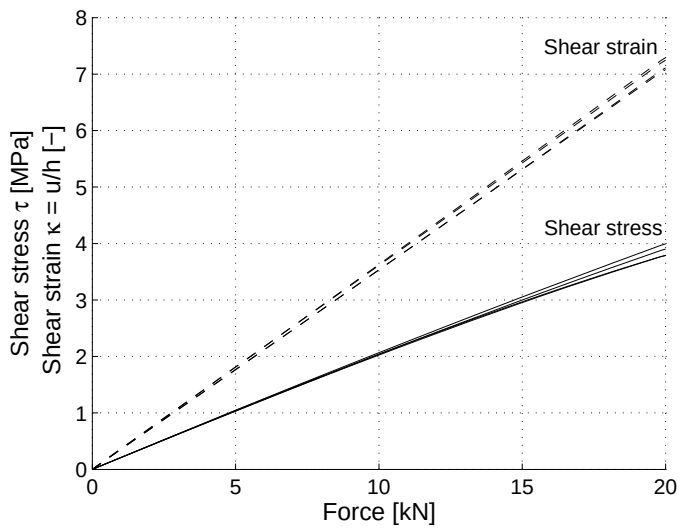

Figure 4.26: *Shear stresses* $\tau = \sqrt{\tau_{13}^2 + \tau_{23}^2}$ *at the integration points of the corner elements and shear strains* κ *in the four corners of the rubber foil for Neo Hooke ultimate limit material model (method 2).*

4.6.3 Discussion

As can be seen in Figure 4.20, the results for the Yeoh and the Neo Hooke models for the serviceability limit state are very close to the test data for load levels of less than 7 kN. This was expected since the models are supposed to be valid for this stress-strain interval. The model for the ultimate limit state developed according to method 1 shows an accurate load-displacement relationship, although with a little too stiff behaviour as can be seen in Figure 4.19. The material model according to method 2 is too compliant, which is expected since the material model was based on a fictitious failure strain which is larger than the actual failure strain.

As can be seen in Table 4.4, the computed ultimate loads for the Neo Hooke material models according to method 1 and method 2 are lower than the experimentally achieved ultimate loads. The reason for the computed failure loads being too low probably inherits from the assumption that complete failure occurs as soon as all four corners of the rubber foil are exposed to strains beyond κ_f. In reality, the redistribution of stresses when the four corners of the foil is torn makes a larger rubber area active for large strains, which increases the load bearing capacity of the joint. Modelling these properties in an FE-analyses is rather complex and was not carried out in this study. Simplified calculations showed that a higher ultimate load is reached when the active rubber area has been decreased from the original rectangular form to an ellipsoidal form. When the ellipsoidal form is reached, the rubber area exposed to strains just below the strain limit κ_c is increased which yields a higher ultimate load [6]. The choice of failure criteria for this calculation is thus not obvious. For example, if a failure criteria based on the shear strain or the shear stress in the integration points of the corner elements would be used, the failure load would be larger than shown in Table 4.4. This can be seen in Figure 4.25 where the failure shear stress ($\tau_f = 3.17$ MPa) at the integration points corresponds to an ultimate load of about 16 kN.

Chapter 5

Application calculations

In the application calculations, a *glued in rod* was analysed in ABAQUS for short term- and long term loading. The loading case pull-pull which is illustrated in Figure 5.1 was used for these simulations. Material properties are described by the material models developed in Chapter 4 and the geometry of the analysed joint can be seen in Figure 5.2.

In short term loading, a parameter study was performed concerning the glued in length of the rod. This parameter is interesting in the evaluation of the rubber's ability to distribute stresses along the rod and thereby increase the load bearing capacity compared to conventionally glued in rods. The purpose of the calculations for long term loading was to study the decrease in load bearing capacity, due to creep, as a function of load duration.

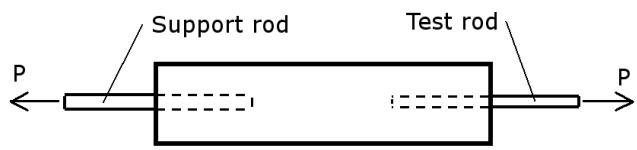

Figure 5.1: *The loading case pull-pull.*

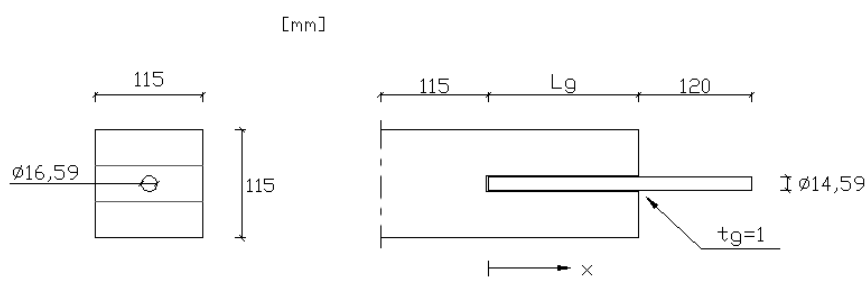

Figure 5.2: *Geometry of the joint.*

5.1 Short term loading

5.1.1 Method

In order to evaluate the influence of the glued in length on the load bearing capacity and the ability of the rubber to distribute the stresses, four models with a rubber foil and different glued in lengths were analysed in ABAQUS. Except from studies of ultimate failure load and stress distribution, the analyses also comprised studies of normal stresses in the rubber foil. The ultimate failure load was defined as the load where the maximum shear strain in the rubber foil reached the failure strain, $\kappa_f = 4.06$, which is obtained in Subsection 3.1.2. This level of strain corresponds to a shear stress of 3.17 MPa.

For the comparison between the stress distribution in a joint with rubber foil and a conventionally glued joint, an analysis of a conventional joint without rubber foil was also made. This analysis was performed for one glued in length and with a simplified material model for the adhesive bond since the purpose was to obtain a stress distribution of principle. Concerning the influence of the glued in length on the load bearing capacity, a comparison between a joint with rubber foil and a joint without rubber foil was also made. In the latter comparison, results from an FE-analysis of a joint without a rubber foil and with similar geometry presented in [5] were used. In that analysis, the diameter of the rod was 16 mm, the cross section of the wood 120x120 mm^2 and the failure stress $\tau_f = 12$ MPa.

For the FE-analyses carried out within this study, the joint was modelled as a quarter of the actual joint by using symmetry in two planes as can be seen in Figure 5.3 which also shows the applied load and boundary conditions. Symmetry was also used in the unloaded end of the model to simulate the loading case pull-pull.

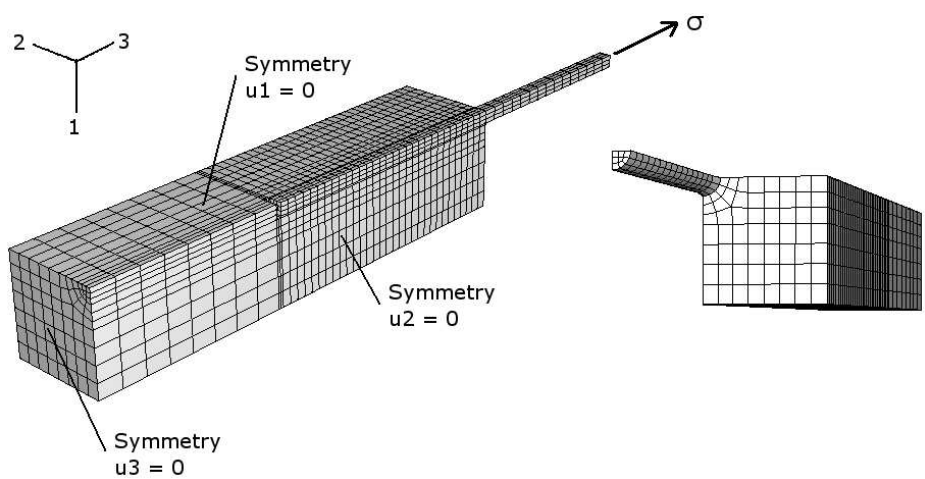

Figure 5.3: *Applied load, boundary conditions and element subdivision for the model.*

The elements used in the calculations were hybrid (mixed formulation), quadratic displacement, 20-node brick elements with 3 degrees of freedom per node (denoted C3D20H in ABAQUS) for the rubber foil and standard, quadratic displacement, 20-node brick elements with 3 degrees of freedom per node (denoted C3D20 in ABAQUS) for the wooden- and steel parts. By experience from FE-analyses performed in Chapter 4, the element subdivision which can be seen in Figure 5.3 was considered fine enough since the size of the elements and expected deformations in the rubber foil are similar to previous analyses.

5.1.2 Materials

Wood

The wooden parts of the joint were modelled as a transverse isotropic material with linear elastic properties according to Table 5.1. Young's modulus E, the shear modulus G and Poison's ratio ν was specified in the three material directions; longitudinal (L), radial (R) and tangential (T) to grain where the material parameters are the same for radial and tangential direction. The difference of the actual parameters in the radial and tangential direction is relatively small and modelling the wood in this way made it possible to use symmetry in two planes.

Table 5.1: *Used material parameters for wooden parts [5].*

Young's Modulus E MPa	Shear Modulus G MPa	Poisson's ratio ν -
$E_L = 14000$	$G_{RL} = 600$	$\nu_{RL} = 0.02$
$E_R = 500$	$G_{TL} = 600$	$\nu_{TL} = 0.02$
$E_T = 500$	$G_{TR} = 60$	$\nu_{TR} = 0.3$

Steel

The steel was modelled as an isotropic material with Young's modulus $E = 210$ GPa and Poisson's ratio $\nu = 0.3$.

Adhesive

Full interaction was assumed between the rubber foil and the wood. The analyses with rubber foil was thus simplified by ignoring the presumably very small deformations in the adhesive bond.

In order to illustrate a stress distribution of principle for a conventionally glued in rod, the stiffness of the foil between the steel and the wood was simply increased with a factor 1000 to represent an adhesive foil instead of a rubber foil.

Rubber

The material model for rubber used in these analyses was the Neo Hooke model according to method 1, described in Section 4.2. Material data for this model is presented in Table 5.2.

Table 5.2: Rubber material data for short term loading.

Neo Hooke coefficient	$C_{10} = 0.3905$	[MPa]
Ultimate shear strain	$\kappa_f = 4.06$	[-]
Ultimate shear stress	$\tau_f = 3.17$	[MPa]
Ultimate normal stress [10]	$\sigma_f = 5$	[MPa]

5.1.3 Results

The strain and stress distribution of the analysed glued in lengths can be seen in Figure 5.4 together with a strain and stress distribution of principle of a conventionally glued in rod. In the figure, both axis are normalised in order to clarify the comparison of the analysed glued in lengths.

Figure 5.5 shows the ultimate failure load and the relationship between applied load and maximum shear strain in the rubber foil for the different glued in lengths. Since the largest strain appears at the free edge of the rubber foil, see Figure 5.4, the maximum strain was measured at this point.

The influence of the glued in length on the load bearing capacity is illustrated in Figure 5.6, which shows the relative decrease in ultimate load for the different glued in lengths compared to the case of perfect stress distribution and the results of an FE-analysis without a rubber foil from [5]. The rubber area is calculated as $A = L_g \cdot \pi \cdot d_m$, where L_g is the glued in length of the rod and d_m is the diameter of the middle of the rubber foil ($d_m = 15.59$ mm).

Figure 5.7 shows the distribution and the magnitude of the normal stresses in longitudinal, radial and tangential direction as well as the shear stress of the centroid of the rubber elements along the length of the rod.

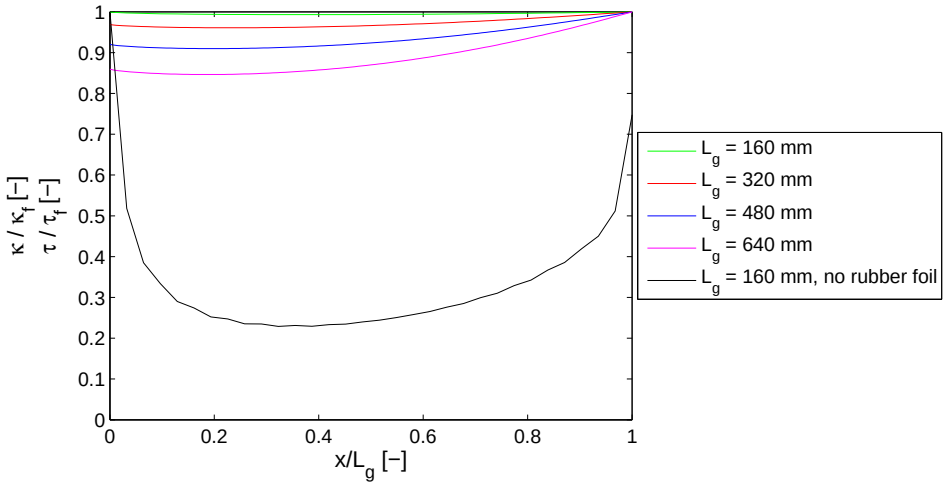

Figure 5.4: *Shear stress and strain distribution in the rubber foil at failure and the corresponding shear stress and strain distribution of a conventionally glued rod.*

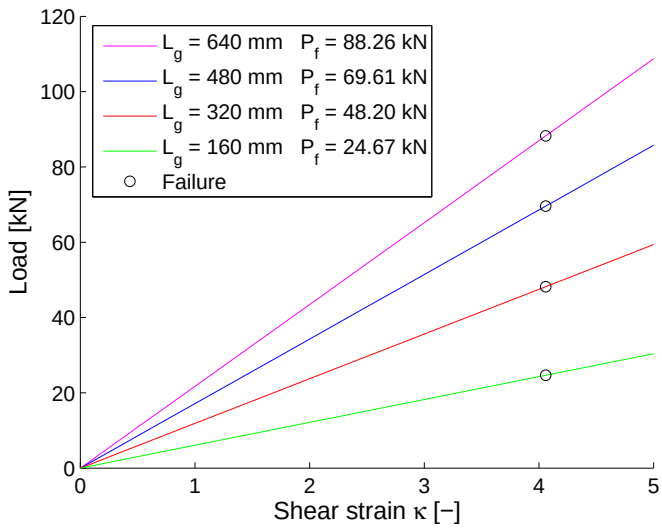

Figure 5.5: *Load vs. maximum shear strain relationships and ultimate loads P_f for the analysed glued in lengths.*

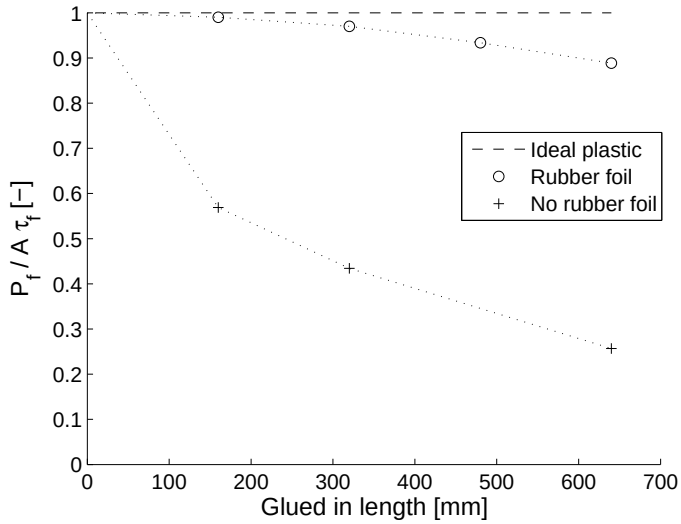

Figure 5.6: *Relative ultimate load vs. glued in length.*

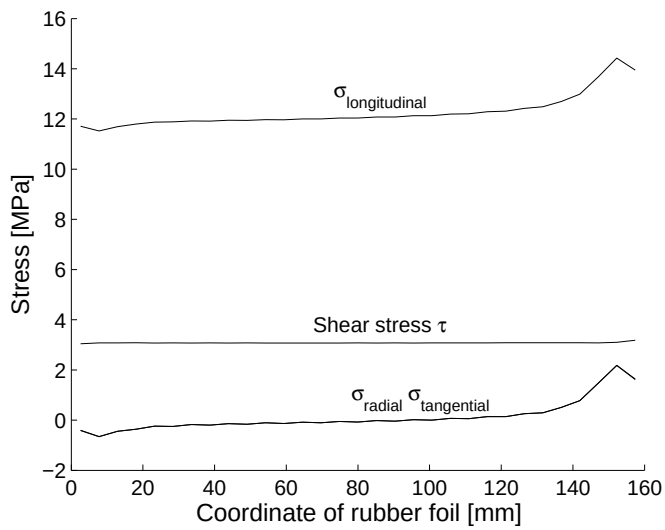

Figure 5.7: *Normal stresses and shear stress in the rubber foil at ultimate load. The glued in length is 160 mm.*

5.1.4 Discussion

The results of this study confirms the anticipation that a rubber foil gives a more uniform stress distribution in a glued joint. As can be seen in Figure 5.4, the shear stress level in the rubber foil is fairly uniform, even for rods of great length. The figure also presents the stress distribution for a short conventionally glued in rod. The large difference in stress distribution of the two types of glued joints is obvious.

In the curve of the conventionally glued in rod, obtained by an FE-analysis, it can be seen that maximum shear stress occurs at $x/L_g = 0$. For stress distributions analytically obtained by one dimensional analysis, the maximum shear stress occurs at $x/L_g = 1$. Independent of how the stress distribution of a conventionally glued in rod is obtained, the difference compared to a rod with rubber foil is however large.

Since the shear stress distribution in the rubber joint is not entirely uniform, the glued in length has some influence on the load bearing capacity. This influence is however very small in comparison with a joint without a rubber foil. This is illustrated in Figure 5.6. The results of the conventionally glued in rod are valid for the failure shear stress $\tau_f = 12$ MPa. This is higher than the assumed failure stress of the rubber foil which is $\tau_f = 3.17$ MPa. The reason for assuming different failure stress was that the rubber used in the work of this thesis is relatively weak. If the rubber had been strong enough to make the capacity dependent on the adhesive bond, full advantage of the rubbers ability to distribute the stresses would have been taken. As a consequence, the capacity would be increased significantly compared to a conventionally glued in rod. For the comparison in Figure 5.6, the failure shear stress is however of less importance since the comparison regards the relative decrease in load bearing capacity.

The study of the normal stresses in the rubber foil showed relatively large stresses at the load level corresponding to the failure strain. Figure 5.7 shows that the maximum normal stress in radial and tangential direction is lower than the ultimate uniaxial normal stress ($\sigma_f = 5$ MPa, [10]). The normal stress in the longitudinal direction is very high, about $12 - 14$ MPa. There is moreover risk for cavitation due to the hydrostatic state of stresses at the free edge of the rod. The hydrostatic normal stress are higher than the cavitation stress of the rubber ($\sigma_{cavitation} \approx 2.5 \cdot G \approx 1.75 < \sigma_{hydrostatic} \approx 2$ MPa).

Large normal stresses in the longitudinal direction is a consequence of the extremely large shear deformation of the rubber foil. As the shear strain increases, the directions of the principle stresses will rotate and approach the longitudinal direction. Normal stresses of this magnitude were most likely also present in the stress vs. strain test since the deformation mode and shear strains are similar. The reason why the rubber can resist larger normal stresses than 5 MPa when exposed to large shear strain is unknown.

5.2 Long term loading

5.2.1 Method

The long term loading properties for a glued in rod were analysed in order to evaluate the time dependency of the load bearing capacity. A shear strain criterion for the serviceability limit state has previously been defined as $\kappa_c = 2.57$ for the CR-rubber, see Subsection 3.1.2. Immediate failure does not occur but it is assumed to be initialised at this strain level.

The analyses of the long term load bearing capacity were carried out with a glued in length of 160 mm. The same FE-model concerning geometry, mesh, boundary conditions and element types as for the short term loading with the same glued in length was used for these calculations.

A critical load P_c which generates an instantaneous shear strain of κ_c was first determined. This load was then decreased by increments of 5 % from $P = P_c$ to $P = 0.7 \cdot P_c$ and the analyses were run over a time period of 10^7 s (≈ 2778 h ≈ 116 days) for each load level. Plotting the increasing shear strain $\kappa(t)$ for each load level generates the time t_c when the critical shear strain κ_c is reached.

5.2.2 Materials

Wood, steel and adhesive

For the wood, steel and adhesive, the same material models as for the short term loading analyses was used, see Subsection 5.1.2.

Rubber

In the choice of material model for the hyperelasticity, the Neo Hooke model was chosen since it generates realistic creep behaviour without having to modify the prony coefficients determining the viscoelastic behaviour as described in Subsection 4.5.2. The used material data developed in Chapter 4 are presented in Table 5.3.

Table 5.3: *Hyper- and viscoelastic material models.*

Hyperelasticity Neo Hooke	$C_{10} = 0.3172$ MPa $\kappa_c = 2.57$	
Viscoelasticity Relaxation modulus $g_R(t)$	g_i [-]	t_{ri} [s]
i=1	0.07255	10^3
i=2	0.04993	10^4
i=3	0.04050	$2 \cdot 10^5$
i=4	0.05397	10^6
$\sum_{i=1}^{4}$	0.2170	-

5.2.3 Expected results

The instantaneous stress vs. strain relationship for a hyperelastic Neo Hooke material is given by:

$$\tau = 2\,C_{10}\,\kappa_e \Rightarrow \kappa_e = \frac{\tau}{2\,C_{10}} \tag{5.1}$$

The increasing shear strain $\kappa(t)$ under a constant shear stress τ can be expressed by the use of the dimensionless relaxation modulus $g_R(t)$ according to:

$$\kappa(t) = \frac{\tau}{2\,C_{10}\,g_R(t)} \tag{5.2}$$

Dividing Equation 5.1 with Equation 5.2 yields:

$$\frac{\kappa_e}{\kappa(t)} = \frac{\frac{\tau}{2\,C_{10}}}{\frac{\tau}{2\,C_{10}\,g_R(t)}} = g_R(t) \tag{5.3}$$

Assume a critical shear strain value κ_c and a Neo Hooke material model. The shear stress giving rise to the critical shear strain κ_c at $t = 0$ is denoted τ_c^0.

$$\tau_c^0 = 2\,C_{10}\,\kappa_c \tag{5.4}$$

The shear stress giving rise to a shear strain of κ_c at a time t is denoted $\tau_c(t)$. Since the shear strain κ varies with time according to the dimensionless relaxation modulus $g_R(t)$ for a constant shear stress, the critical shear strain κ_c will be reached at different times for different constant shear stresses.

$$\tau_c(t) = 2\,C_{10}\,\kappa_c\,g_R(t) \tag{5.5}$$

Dividing Equation 5.5 with Equation 5.4 yields:

$$\frac{\tau_c(t)}{\tau_c^0} = \frac{2\,C_{10}\,\kappa_c\,g_R(t)}{2\,C_{10}\,\kappa_c} = g_R(t) \tag{5.6}$$

The distribution of stresses and strains will be the same for all levels of the external load since the Neo Hooke material model is linear for simple shear. If the external load is doubled, the distribution of stresses and strains will be the same but the magnitude of the stresses and strains will be doubled in every point of the material. For a material with a homogeneous stress distribution, the ratio between long term critical load and the short term critical load will vary with time according to the dimensionless relaxation modulus $g_R(t)$.

$$\frac{P_c(t)}{P_0} = g_R(t) \tag{5.7}$$

If the relative stiffness between the involved materials are changed, the stress distribution while also change. In these FE-analyses, relaxation is only specified for the rubber while the stiffness of the wood and the steel are kept constant. Hence, the stress distribution in the rubber foil will change over time. This change in stress distribution is however small and the decrease of the relative load bearing capacity can therefore be approximated according to Equation 5.7.

5.2.4 Results

The used loads P_i and corresponding instantaneous shear strains κ_e and times t_c when the critical shear strain κ_c are reached are presented in Table 5.4. The increasing shear strains $\kappa(t)$ for the different load levels are shown in Figure 5.8 for the complete calculation time and in Figure 5.9 for the first 500 hours. Figure 5.10 shows the dimensionless relaxation modulus and the ratio $\kappa_e/\kappa(t)$ for the different load levels.

Table 5.4: *Results of FE-analyses for a glued in length of* $L_G = 160$ *mm.*

i	P_i [kN]	P_i/P_0 [%]	κ_e [-]	t_c [s]	t_c [h]
0	12.69	100	2.57	instant	instant
1	12.05	95	2.44	2830	0.786
2	11.42	90	2.31	9970	2.77
3	10.79	85	2.18	$1.66 \cdot 10^5$	46.1
4	10.15	80	2.06	$1.52 \cdot 10^6$	423
5	9.52	75	1.93	-	-
6	8.88	70	1.80	-	-

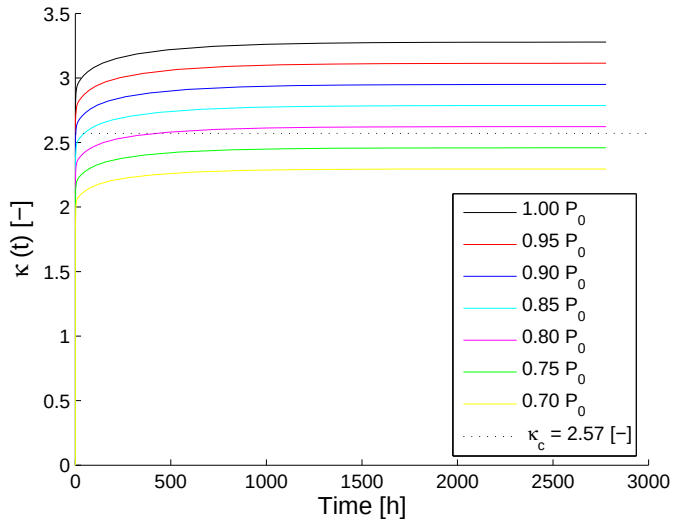

Figure 5.8: *Shear strain $\kappa(t)$ for different load levels.*

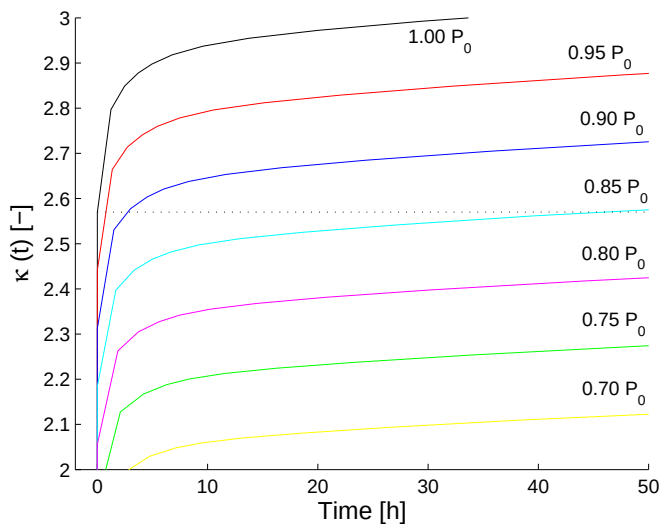

Figure 5.9: *Shear strain $\kappa(t)$ for different load levels.*

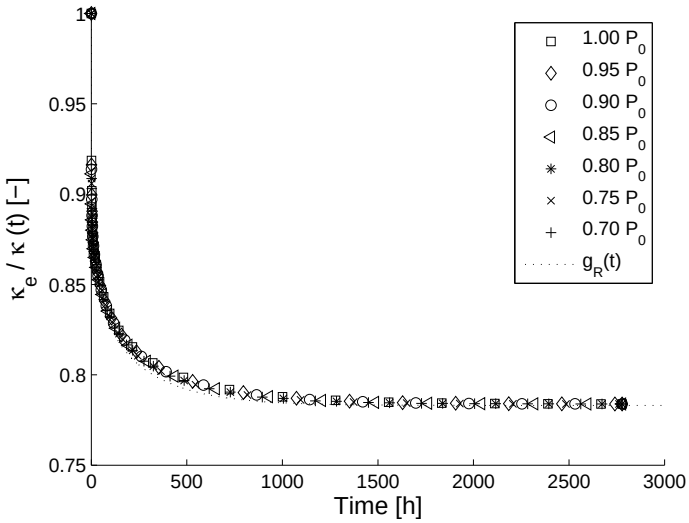

Figure 5.10: $\kappa_e/\kappa(t)$ *for different load levels.*

Figure 5.11 and Figure 5.12 show the dimensionless relaxation modulus and the ratio $P_c(t)/P_c(0)$ for the different load levels in different time scales.

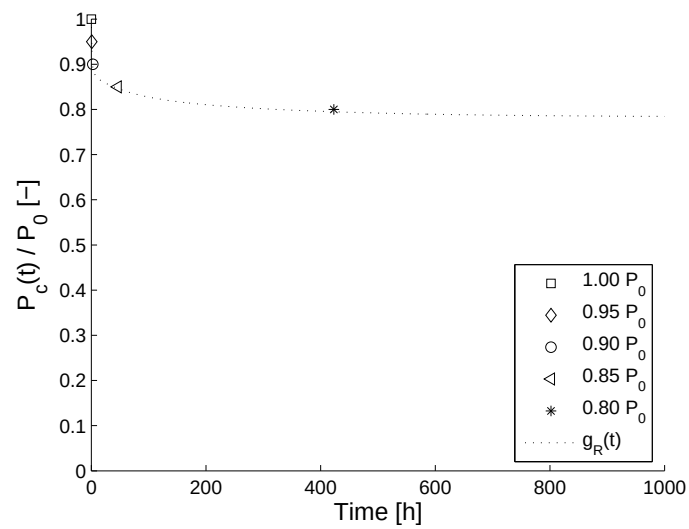

Figure 5.11: $P_c(t)/P_c(0)$ *for different load levels.*

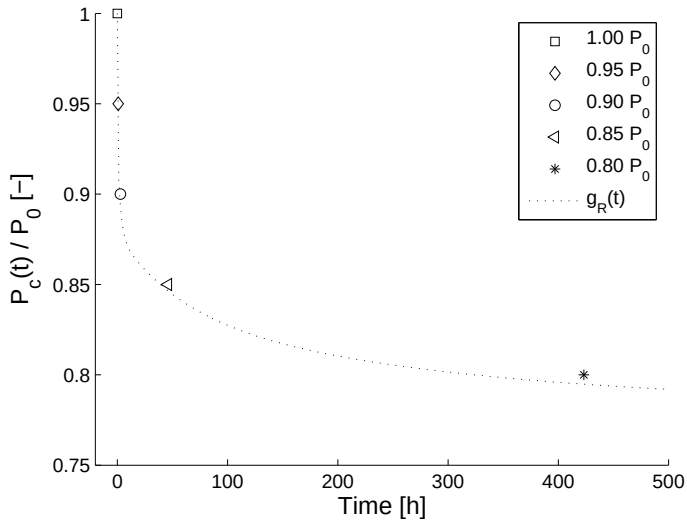

Figure 5.12: $P_c(t)/P_c(0)$ *for different load levels.*

5.2.5 Discussion

The FE-analyses show that the load bearing capacity is decreased significantly for long duration of load compared to short term loading. Since the creep rate is high for the first hours, see Figure 5.9, the decrease in capacity is also large within this time span. The decrease in load bearing capacity is thus to a large extent dependent on choice of time at which the deformation in the experimental tests is regarded as instantaneous. For example, if the instantaneous deformation would be defined as the deformation after four hours, the decrease in capacity after 3000 hours would be half of the decrease in Figure 5.9. As mentioned in Subsection 3.4.2, the instantaneous deformation in the development of the viscoelastic material models in this thesis is defined as the deformation one minute after loading.

As can be seen in Figure 5.10 - 5.12, the results of the calculations are very close to the curve of the dimensionless relaxation modulus. The small difference between the calculation results and $g_R(t)$ is probably caused by the change in stress distribution over time. As the stiffness of the rubber decreases, the stress distribution will become more uniform and the difference between the calculation results and $g_R(t)$ decreases, as can be seen in Figure 5.10. Thus, the theory presented in Subsection 5.2.3 seems to be correct.

Chapter 6

Concluding remarks

6.1 Conclusions

The work of this master's thesis has resulted in many conclusions which are discussed in the discussion-subsections appearing in the sections of each separate test or analysis. In this chapter, some of the conclusions regarded as the most important are discussed.

The main idea of using a rubber foil in a glued joint is to increase the load bearing capacity by taking advantage of the rubber's ability to distribute stresses along the glued in length of the rod. In terms of fracture mechanics, this ability is due to the extremely high fracture energy of the rubber foil. In Section 5.1 it is shown that the idea of distribution of stresses holds very well. By using a rubber foil, the large concentrations of stresses which limit the capacity of conventionally glued in rods are avoided. The uniform stress distribution also yields only a small loss of relative load bearing capacity with increasing glued in length compared to conventionally glued in rods.

Despite the uniform stress distribution, the load bearing capacity obtained from FE-analyses is not higher than a traditionally glued in rod with the same geometry. This depends on the used CR-rubber being to weak. In order to take full advantage of the ability to distribute stresses, a stronger rubber should be used to assure that failure occurs in the adhesive bond or the wood. A possibility to decrease the deformations could be to use a stiffer rubber. This would however result in a less uniform stress distribution.

For long term loading, it is shown in Section 5.2 that the load bearing capacity is determined by the viscoelastic properties of the used rubber. The load bearing capacity decreases over time according to the decrease of the stiffness of the rubber. For a rubber that can be well described by a linear stress vs. strain relationship in simple shear, this decrease in stiffness can be described by the dimensionless relaxation modulus. In Section 5.2 it is also shown that the load bearing capacity decreases significantly over time in the case of long term loading. The decrease in load bearing capacity is however to a large extent dependent on the choice of time (in the development of the material models) at which the deformation in the

experimental tests is regarded as instantaneous.

In the work of developing a material model it turned out to be difficult to find a single exhaustive hyperelastic model. Several models were instead developed, with validity for various stress levels, in order to be able to perform calculations on different kinds of applications.

6.2 Proposals for future work

The difficulties faced during the work of this thesis have resulted in some ideas that probably can be of use for future work in this area. In this section, these ideas are presented.

- Investigation of available rubber qualities that are stronger than the rubber used in the work of this thesis.
- Short term experimental tests of the stronger rubber quality in order to develop a hyperelastic material model. These tests should if possible contain more specimens than the tests analysed in this study.
- Long term experimental tests of the stronger rubber quality in order to develop a viscoelastic material model. The tests should be more extensive than the creep tests included in this thesis, suggestively with more test specimens for each load level loaded under a longer time period before analysing the test data.
- An idea for future experimental testing is to use test specimens consisting of steel and rubber only. In this way, the work of considering strains in the wooden parts would be avoided and it would be easier to develop accurate material models valid for the rubber only.
- If possible, develop material models for the rubber that can describe the entire course of events, from zero stress to ultimate failure stress. By obtaining this kind of material model, it would not be necessary to have separate models for FE-analyses in serviceability- and ultimate limit state. In order to obtain an exhaustive material model it would be necessary to describe the properties of the rubber beyond the second inflexion point of the stress-strain relationship. This might be possible by taking into account the assumed changes in microstructure that occur at a certain strain level, in this thesis defined as the serviceability limit, see Figure 2.13.
- Investigate the possibilities of developing a more sophisticated failure criteria.
- Application calculations of different kinds of glued in joints in order to further investigate the possibilities of glued rubber foil timber joints.

Bibliography

[1] Austrell P.-E., Bellander M., Stenberg B., Carlsson U., Kari L., and Persson S., *Survey of design methods and material characteristics in rubber engineering*. Report TVSM-3036, Lund University, Division of Structural Mechanics 1998.

[2] Austrell P.-E., *Modeling of elasticity and damping for filled elastomers*. Report TVSM-1009, Lund University, Division of Structural Mechanics 1997.

[3] ABAQUS INC., *ABAQUS getting started manual* Version 6.4 2003.

[4] ABAQUS INC., *ABAQUS Analysis user's manual, Volume III: Materials* Version 6.4 2003.

[5] Gustafsson P.-J. and Serrano E., *Glued in rods for timber structures - Development of a calculation model*. Report TVSM-3056, Lund University, Division of Structural Mechanics 2002.

[6] Gustafsson P.-J., *Personal communication* 2005.

[7] Hibbit, Karlsson and Sorensen, *ABAQUS Theory manual* Version 5.8 1998.

[8] Malvern L.E., *Introduction to the Mechanics of a Continous Medium*, Prentice-Hall, 1969.

[9] Wikström M., *Studies of Rubber-based Joints in Laminated Wood*. Master's thesis, KTH Stockholm, Department of Chemistry 2005.

[10] Trelleborg Industri AB, *Gummiduk*. Article # 187510, JMS Mediasystem, 2004.